

DEVELOPMENT OF AN APPARATUS FOR
FATIGUE UNDER HYDROSTATIC PRESSURE

by

Kjell Lövold

ProQuest Number: 10781664

All rights reserved

INFORMATION TO ALL USERS

The quality of this reproduction is dependent upon the quality of the copy submitted.

In the unlikely event that the author did not send a complete manuscript and there are missing pages, these will be noted. Also, if material had to be removed, a note will indicate the deletion.



ProQuest 10781664

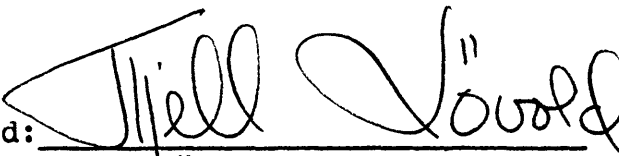
Published by ProQuest LLC (2018). Copyright of the Dissertation is held by the Author.

All rights reserved.

This work is protected against unauthorized copying under Title 17, United States Code
Microform Edition © ProQuest LLC.

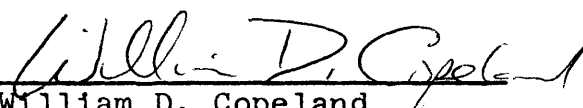
ProQuest LLC.
789 East Eisenhower Parkway
P.O. Box 1346
Ann Arbor, MI 48106 – 1346

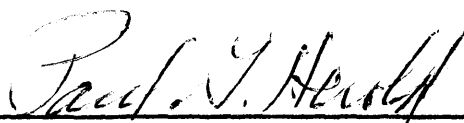
A Thesis submitted to the Faculty and the Board of Trustees of the Colorado School of Mines in partial fulfillment of the requirements for the degree of Master of Science.

Signed: 
Kjell Lövold

Golden, Colorado

Date: December 11, 1969

Approved: 
William D. Copeland
Thesis Advisor


Paul G. Herold
Head of Department
Metallurgical Engineering

Golden, Colorado

Date: Dec 13, 1969

ABSTRACT

An apparatus for fatigue under hydrostatic pressure was designed and built. It was tested successfully with oil as the pressure medium and for pressures up to 10,000 psi. Reverse bending tests were run with cold rolled copper samples. A significant increase in the fatigue life of the specimens was found when the pressure was increased up to 10,000 psi. This was attributed to a slowing down of the propagation of cavities and microcracks due to the compressive stresses set up by the hydrostatic pressure.

TABLE OF CONTENTS

	Page
ABSTRACT	iii
LIST OF FIGURES.	v
LIST OF TABLES	vii
ACKNOWLEDGMENTS.	viii
INTRODUCTION	1
LITERATURE SURVEY.	2
THEORY	6
APPARATUS AND EXPERIMENTAL PROCEDURE	13
Pressure Vessel	13
Closure	13
Electrical Connection	15
High Pressure System.	16
Bending Apparatus	17
Electrical System and Counting Mechanism.	19
EXPERIMENTAL RESULTS	32
DISCUSSION OF EXPERIMENTAL RESULTS	39
SUMMARY AND CONCLUSIONS.	41
SUGGESTIONS FOR IMPROVING THE APPARATUS AND FOR FURTHER WORK	42
APPENDIX I: Calculation of Stresses in the Test Specimen.	44
APPENDIX II: Design of the Pressure Vessel.	56
APPENDIX III: Statistical Treatment of Fatigue Data in Air and Oil Under Atmospheric Pressure	63
BIBLIOGRAPHY	65

LIST OF FIGURES

Figure	Page
1. Schematic figure of motor torque	18
2. Pressure vessel and closure.	24
3. Cone connection for electrical leads	25
4A. Schematic view of connection for high pressure tubing.	26
4B. High pressure arrangement.	26
5. Schematic figure of the bending mechanism.	27
6. Schematic figure of the electrical arrangement	28
7. Schematic figure of the electronic counter	29
8. General layout of the apparatus.	30
9. Detail of main parts of the apparatus.	31
10. Relation between cyclic stress and fatigue life for the test piece under three different oil pressures.	33
11. Relation between cyclic stress and fatigue life for the test piece in air and oil at atmospheric pressure	34
12. Lifetime of a test piece being subjected to a cyclic stress of 60,500 psi under three different pressure combinations.	35
13.-20. Figures to illustrate the calculation of stress in the test piece.	44-50
21. Test piece	54
22. Relation between maximum stress and deflec- tion for a copper test piece	55

Figure	Page
23. Section through the pressure vessel.	56
24. Stress distribution through the vessel wall. . .	59

LIST OF TABLES

Table	Page
1. Fatigue data for tests in oil under three different pressures	36
2. Comparison of fatigue data in oil and air under atmospheric pressure.	37
3. Fatigue data for tests in oil at a 60,500 psi stress amplitude.	38

ACKNOWLEDGMENTS

The author wishes to express his gratitude to Dr. W. D. Copeland for his guidance in the preparation of this thesis.

The author also wishes to thank Mr. Jack Kintner for his work in machining the pressure vessel.

Thanks are also expressed to the Colorado School of Mines Foundation for providing financial support to the author for the duration of this study.

INTRODUCTION

In recent years there has been increasing activity in the exploration of the deep oceans and the ocean bottom. However, we have a very limited knowledge about how engineering alloys will behave under such conditions. That is, we know very little about how the pressure will cause changes of the mechanical properties of metals and how the corrosive properties of sea water will affect metals as a function of water pressure, temperature, gas content, salinity, and time. At present no mechanical studies have been conducted in a deep ocean environment, and relatively few investigations have been done on a laboratory scale.

The object of this study was to design, build, and test an apparatus which could be used to make fatigue tests under hydrostatic pressure up to 10,000 psi. Only the pressure effect was to be studied, so oil was used as the pressure medium. The fatigue apparatus was built for reverse bending and the test pieces which were used were made of cold rolled copper.

LITERATURE SURVEY

Very little has been done in the field of fatigue under hydrostatic pressure, and only a couple of valuable publications have been found.

Rowland, DeVries, and Gibbs (1967, p. 131) made rotating beam fatigue tests for pressures up to 100,000 psi. Test specimens were Fe, Al, and Ni-wires, and a significant increase in life time was observed for increasing pressures. The effect of pressure was found to be greater, the smaller was the strain amplitude. Pressurization at 100,000 psi prior to fatigue tests at atmospheric pressure increased the fatigue life slightly. It was also found that samples run at atmospheric pressure for the first few percent of their lifetime and at 70,000 psi for the remaining life showed a decreasing lifetime with respect to the expected lifetime they would have if they had been at high pressure all the time. It was therefore concluded that the nucleation of cracks, which occur early in the fatigue life, exhibits a much stronger pressure dependence than the propagation of cracks.

Burns and Parry (1964, p. 293) made reverse torsion fatigue tests in oil under a pressure of 40,000 psi and with specimens made of 2.5 percent nickel-chromium-molybdenum steel. Provided that the surface was protected from the

fluid by a rubber coating, an average increase in the fatigue life of 30-40 percent was observed. Because without the protective rubber coating the fatigue life was lower, it was concluded that oil under high pressure had a deliterious effect on the surface of the specimen.

In a field closely related to fatigue, it is reported that the ductile-brittle transition temperature for recrystallized powder metallurgy molybdenum has been lowered from 50°C to 2°C by the application of a hydrostatic pressure of 20,000 psi (Galli and Gibbs, 1964, p. 774). It was also reported that the increase in the fracture stress was the same as the increase in hydrostatic pressure.

Asai and Hayes (1957, p. 138) have shown that when tested in an environment of high hydrostatic pressure a brittle material as chromium may show ductility.

However, a few interesting irreversible effects also occur in metals which have been subjected to high hydrostatic pressure.

Bullen, Henderson, Wain, and Paterson (1964, p. 803) have shown that brittle chromium is ductile not only while under high hydrostatic pressure, but also at atmospheric pressure after being subjected to a hydrostatic pressure of 150,000 psi for five minutes. Strains up to 60 percent were needed before fracture occurred; this was at a strain rate of 10^{-3} per min. It was suggested that the effect is due to the appearance of free dislocations at elastic inhomogeneities

during pressurization. The yield stress for pressurized chromium was found to be approximately half of the brittle fracture stress of recrystallized chromium. The pressurized specimens became brittle after aging at 450°C or higher temperatures.

Bullen, Henderson, Hutchison, and Wain (1964, p. 285) showed that for Armco iron (3 percent C, S, Ni; 8 percent Mn) the yield point is substantially reduced in specimens subjected to hydrostatic pressure in the range of 100,000 psi prior to the tests. This was explained by the free dislocations which were created during pressurization at elastic inhomogeneities as inclusions or as a second phase. This was supported by the fact that high purity iron was not affected by the high pressure.

Findley and Tracy (1966, p. 1479) made ultrasonic measurements in polycrystalline and single-crystal copper which were subjected to pulsating hydrostatic pressure up to 40,000 psi. The measurements were made after pressurization, and it was found that after each cycle the attenuation in polycrystalline copper was increased. This was attributed to shear stresses set up by inhomogeneities in the metal and by anisotropy of the elastic constants. Such irregularities could generate dislocations and cause breakaway of dislocation loops which would increase the attenuation. (Attenuation was considered as a linear function of the dislocation density.) A decrease in the attenuation in single crystal

samples was found. This was explained by the assumption that vacancies migrated to the surface and dislocation pairs would have an increased tendency to annihilate each other because of the high hydrostatic pressure.

For information about ordinary fatigue under atmospheric condition, one may refer to a book on metal fatigue by Sines and Waisman (1959), to Wood et al.'s publication on systematic microstructural changes peculiar to fatigue deformation (1963), and to the proceedings of the First International Conference on Fracture, Japan, 1966.

THEORY

The mechanism for fatigue can be divided into two parts: One for the low cycle region where we have large amplitudes and plastic deformation in the test piece, and one for the high cycle region where we have small amplitudes and no plastic deformation.

For a bending test the stress distribution across the cross-section of the test piece varies as shown in figure 16 in Appendix I. For bending downwards, for example, there is maximum compression in the lower fibers, zero stress in the neutral axis, and maximum tension in the upper fibers. Therefore, even for maximum bending amplitudes there is still a region near the neutral axis which operates within the elastic range. Consequently, both mechanisms are working in the low cycle region.

Considering our copper specimen which has a yield point of around 32,000 psi (ASTM Handbook, 1954, p. 300), we should be in the low cycle region when the fatigue life of the specimen is less than 150,000 cycles. This can be seen from figure 11 (32,000 psi correspond to 150,000 cycles).

For copper the two fatigue mechanisms have been described by Wood et al. (1963, p. 643). In the low-cycle region there are plastic deformations and each grain is broken down into small regions of different lattice

orientation separated by irregular sub-boundaries of distortion and internal strain. After 1/200 of the specimen's life small pores appear on the sub-boundaries and they multiply and coalesce into cavities. There again multiply and link into micro-cracks. Finally when the latter are numerous enough they link into irregular cracks which extend beyond the grain boundaries, and macroscopic failure soon follows. A significant feature is that the microcracks develop early in the life of the test piece and they stay within the grains for the greater part of the remaining life. As the number of cycles increases, more pores combine and form cavities which again will form micro-cracks, but these processes are confined within the grain boundaries.

In the high cycle region there are small strains in the test piece and fatigue develops in a reasonably ordered structure. We get a combination of forward and backward slips and cross-slip to other slip planes. As a result we get zones of structural disturbance within the grains, and at the surface of the specimen these will appear as very small extrusions or intrusions. These zones are observed after only 1/1000 of the lifetime, and as soon as they are formed they become the sites of small pores. As the number of cycles increases, the pores multiply; they coalesce into cavities which finally disintegrate into the zones along their whole length and we get fatigue zones. At last, as the fatigue zones multiply, they cross-link to make the

structure collapse; macrocracks are formed and failure starts. The fatigue zones also emerge to the surface and peaks and cracks are formed along them.

In both these mechanisms small pores are formed as early as the first 1/200 of the specimen's lifetime, and after this period it is not structurally sound any longer (Wood et al., 1964, p. 645). The pores may be formed by moving dislocations which sweep up vacancies and move them to suitable sinks such as grain and sub-grain boundaries or irregularities within the grains (Kochendorfer, 1954, p. 351). Or, these vacancies will diffuse to dislocations on other lattice imperfections and relieve the stress field around them.

High pressure should have an effect on the mechanisms which have been described. With respect to the movement of dislocations the Peach-Koehler equations (Weertman and Weertman, 1964, p. 61) show that the forces acting on a dislocation are governed by shear stresses only except for the climb of edge dislocations, which depends upon tensile or compressive stresses. Since the hydrostatic pressure has no influence on the shear stresses, one should expect that it has an effect on edge dislocations only. However, a modified form of this equation has been proposed by Weertman (1965, p. 1217); it predicts that hydrostatic pressure produces no net force on any dislocation.

The vacancy concentration plays an important role in

fatigue, as mentioned earlier, and in equilibrium it is given by (Weertman and Weertman, 1964, p. 75):

$$X_v = \exp \left(\frac{TS_v - pV - Q_v}{kT} \right) \quad (1)$$

where

k = Boltzmann's constant

S_v = change in entropy per vacancy created

Q_v = energy of formation of one vacancy

T = temperature in $^{\circ}\text{K}$

V_v = volume of a vacancy

p = pressure

The diffusion in metals is also pressure dependent, and according to DeVries et al. (1963, p. 2254), the self diffusion coefficient can be written as

$$D = D_0 \exp \left(- \frac{p\Delta V}{kT} \right) \quad (2)$$

where

D_0 = diffusion coefficient at zero pressure

ΔV = activation volume = $\Delta V_v + \Delta V_m$

ΔV_v is the volume of a vacancy, and its magnitude will depend on the degree to which surrounding atoms relax into it. In copper, ΔV_v is approximately 55 percent of the volume of one copper atom (Shewmon, 1963, p. 83). The second term contributing to the activation volume, ΔV_m , is the change in atomic volume in the activated complexes. That is, this is the change in atomic volume when an atom jumps from one

position to another and passes through the saddle point between the two positions. Shewmon gives a ΔV_m -value which is around 9 percent of the volume of one copper atom. Thus, the activation volume is positive and is approximately 64 percent of the copper-atom volume.

It can be seen that both the vacancy concentration and the diffusion coefficient will decrease with increasing pressure, a fact which implies that the formation of pores is made more difficult. If this is significant, we should then expect an increase in the lifetime with increasing hydrostatic pressure. However, if this is the only factor being affected by the hydrostatic pressure, it will be difficult to detect the effect since this crack-initiation stage lasts for only a few percent of the total lifetime. For example, if the crack initiation takes place in the first 2 percent of the lifetime and we get an increase of 100 percent of this stage, the total lifetime of the sample will increase with 2 percent only. But, this can hardly be detected because of the data scattering.

The hydrostatic pressure should also have the effect of squeezing cavities and microcracks together so that they will have more difficulties in linking together and moving through the grains. This effect should also have the tendency of increasing the fatigue life.

If a test piece is run under atmospheric pressure in

the first 5 percent of its expected lifetime, many pores and cavities are formed by the end of this period. This process depends upon the vacancy concentration and the diffusion of vacancies. If the hydrostatic pressure is increased for the rest of the lifetime, we will be at the stage where cavities link and microcracks are formed, and there again run together and form macrocracks.

Therefore, if the hydrostatic pressure has its main effect on the propagation of cavities and microcracks, the lifetime of the test piece should approximately be the same as for samples where hydrostatic pressure was applied all the time. On the other hand, if the hydrostatic pressure has an effect only on the vacancy concentration, the diffusion of vacancies and the formation of pores, and not on the propagation of microcracks, the lifetime of the sample should be the same as for samples where no hydrostatic pressure was applied at all. However, if the pressure has an effect on both stages, the lifetime would essentially be the same as for samples under hydrostatic pressure all the time. This can be explained by the fact that since the crack initiation stage takes up a so small percent of total lifetime, an increase in this stage from 50 to 100 percent can hardly be detected because of the data scattering. Thus, these tests can tell us whether or not the pressure has an effect on crack propagation, but it will be difficult

to tell what effect it has on crack nucleation, unless we get an increase of several hundred percent of this stage.

APPARATUS AND EXPERIMENTAL PROCEDURE

Pressure Vessel

The pressure vessel is shown in figure 2. It is shown in Appendix II that the vessel can support an internal pressure of 15,200 psi before the metal in the inner part of the cylinder wall reaches its limit of elastic behavior. And, since the stresses decrease with increasing distance from the cylinder axis, we will be further and further away from the elastic limit as we are going from the inner to the outer wall. Even if we reach this limit for the metal fibers in the inner wall, we are still very far from the tensile strength which is at least 80,000 psi. It was therefore considered safe to go to internal pressures up to 15,000 psi. This was done in order to test the pressure vessel, and no sign of plastic deformation was observed. It should also be mentioned that the corners in the bottom of the pressure vessel were rounded off in order to avoid any notch effect.

Closure

The pressure vessel was closed with a Bridgman-type closure (Comings, 1956, p. 105), based on his principle of the unsupported area (Bridgman, 1952, p. 32) - see figure 2. It works in the following way: First, the floating head, two gaskets of aluminum and teflon, and the brass cylinder

with the bending apparatus are lowered into the pressure vessel. Then the cap ring is screwed in and the thrust ring is screwed onto the floating head. The six socket head bolts on the thrust ring are fastened, and this makes certain that the floating head is pressed upwards. Because of this, the teflon gasket is squeezed together and also pressed out radially against the wall by Poisson's effect to make the initial seal. This is also helped by the fact that the aluminum gasket is tapered off 5° towards the wall to give the teflon gasket an extra tendency of squeezing out radially.

Later on when the pressure is increased, the force acting on the bottom of the floating head (the unsupported area) and tending to blow it out is transmitted to the cap ring through the gasket. Since the gasket area is smaller than the unsupported area, the pressure exerted by it must be larger than the hydrostatic pressure in the vessel. The closure was designed so that the area of the bottom of the floating head was approximately twice as large as the gasket area. Therefore, for any fluid pressure, the hydrostatic pressure in the gasket will be twice as large as the fluid pressure, and no leak will occur as long as the gasket remains soft.

Initially, different rubber gaskets were tried and the seal worked perfectly. However, they squeezed out along the

wall for pressures above 5,000 psi, and this made the opening of the closure difficult. (A 2-ft wrench had to be used in order to unscrew the cap ring.) These rubber gaskets were also so easily destroyed by the "squeezing out" that they could be used only a few times.

The best gasket material is teflon. It squeezed out very little, it did not hinder the opening of the closure, and the same gasket was used more than 50 times without any observable deterioration.

Because of the large forces acting on the closure, it was made of 4340 steel which was heat-treated to a hardness of 43 RC (ASME Handbook, 1954, p. 231). This corresponds to a yield point of 190,000 psi and a tensile strength of 200,000 psi.

Electrical Connection

In order to get the electrical circuits into the pressure vessel, a modified type of Amalgat's cone connection was used (Bridgman, 1952, p. 52) - see figure 3. Holes were drilled longitudinally through the floating head; and in the bottom of the latter, hollow 60° cones were drilled. These were used as sites for brass cones with insulated electrical leads soldered onto the bottom. Impact resin supported by nylon cloth was used as insulation and seal between the floating head and the brass cones. Thus, as the pressure increased the brass cones were pressed into the hollow cones.

This cone connection was useful as long as there was no electrical contact between the floating head and the brass cones. The upper pressure limit for which this type is useful was determined from the insulating material's resistance to flow. It was noted that this connection type was useful up to around 45,000 psi.

Several tests were made on a tensile machine, and it was found that with a combination of impact resin and nylon cloth as insulation an axial pressure of 110,000 psi (or 250% above what has been reported) was needed before the insulation broke down and electrical contact was established between the brass cone and the floating head.

High Pressure System

The fluid used in the high pressure system was Texaco Aircraft Hydraulic Oil AA. The 1/4-in.-O.D. and 1/16-in.-I.D. tubing used to transmit the oil pressure from the pump to the pressure vessel was made of 316 stainless steel. This arrangement is shown in figure 4B. The connection to pressure vessel, elbow and pump is shown schematically on figure 4A. The tubing collar is screwed on the tubing, and the gland nut presses the tubing into a 60° cone when it is tightened. Since the end of the tubing is coned to an angle of 59°, there will be a metal-to-metal line contact between the tubing and, for example, the pressure vessel. This connection worked perfectly and there was no sign of any leak.

The tubing and the different parts used in this connection were bought from Harwood Engineering, Massachusetts.

The Sprague pressure pump is air operated and gives an output oil pressure which was fairly constant and would not fluctuate more than 5% from the desired pressure level.

For long lasting tests the equilibrium temperature in the vessel was 39°C. If the oil temperature was lower than that when the test started, the oil would be heated up by the motor and thus make the pressure increase and be greater than desired. It was therefore required in some cases to open the bleed valve to release the pressure so that it dropped down to correct value.

For safety reasons the pressure vessel was mounted behind an iron shield. However, no failure occurred during the experiments.

Bending Apparatus

The bending apparatus is shown schematically in figure 5. It is mounted in a brass cylinder, and the rotating movement of the motor is transmitted through a pair of gears to a fly wheel. The arm doing the bending is attached to an eccentric axis on the fly wheel. Thus the bending amplitude depends on the eccentricity of this axis. The eccentric has a calibrated scale, and in the experiments the bending amplitudes varied from 1.25 to 5.50 mm.

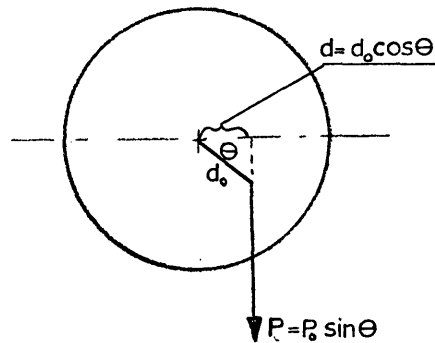


Figure 1.

We will consider the eccentric with bending amplitude $d_0 = 6$ mm as shown in figure 1. As shown in Appendix I, a force $P_0 = 37$ N is needed to complete this bending. From the figure we see that the torque is given by

$$M = P_0 d_0 \sin\theta \cos\theta = \frac{P_0 d_0}{2} \sin 2\theta \quad (3)$$

We have a maximum torque of $M_0 = 1/2 P_0 d_0 = 0.111$ Nm for $\theta = 45^\circ$. Exaggerating and assuming that this is the constant torque during the whole rotation, we find that the power W needed in order to make the rotation is given by

$$W = M_0 \omega \quad (4)$$

This is in the S.I. system, and ω is the motor speed in radians per second. It was desired to have a high number of rotations per minute, so that the tests could go fairly fast. Using a motor with 3000 rpm or $\omega = 2\pi \times 50$, we find that the maximum power needed is 35w or around 0.05 Hp.

The motor chosen was a Dayton shaded pole type, 0.067 Hp

and 3000 rpm. The shaded pole motor has the advantage that there are no brushes between rotor and starter (these will wear out and contaminate the pressure medium), and the rotor has a smooth, cylindrical surface which makes minimum friction with the fluid when it rotates. In oil at atmospheric pressure the motor had a speed of 3420 rpm when there was no load on it. With maximum load and at 10,000 psi hydrostatic pressure the speed was 3000 rpm. However, the motor would not start if the eccentric was regulated for maximum load and the test piece was in zero position ($\theta = 0$). The flywheel had therefore to be rotated so that the test piece was in maximum deflection position ($\theta = 90^\circ$). Now, no torque was applied to the motor, and the force in the test piece trying to get it back to zero position helped the motor to start.

Electrical System and Counting Mechanism

The electrical system is shown schematically in figure 6. The DC current from the batteries to the electronic counting mechanism and the AC current to the counter and the motor go through the relays 1 and 2. These two are activated by a current going through the test piece so that when it breaks everything will stop. This particular circuit goes to the pressure vessel itself (which is grounded), then through the bending arm to the test piece. This one is insulated from the pressure vessel at the base (figure 5)

and the current is taken out from this part through one of the cone connections and to the coil of each relay.

Originally, the plan was to use two 12V DC-relays, but it turned out that when the motor was running, DC current could not pass through the ball bearings in the bending arm, which were the only contact points between ground and the arm.

Fortunately, it was discovered that 120V AC could pass through, and relays for this current type were therefore used.

This method of stopping the motor and the counter worked very satisfactorily for small bending amplitudes. For the largest bendings, however, the two broken pieces smashed into each other for each rotation of the eccentric and thus reestablished electrical contact. In this way the motor and the counter would go on, though very irregularly. But for these large amplitudes each test took a few minutes only, so the relays could be switched off manually since one could easily hear when the test piece broke.

In order to count the number of bendings, which was the same as the number of rotations of the motor, a piece of permanent magnet was cast in an impact resin cylinder on the motor axis and a pick-up coil of 500 windings and soft iron core was placed next to it (figure 5). For each rotation or for each time the magnet passed by the coil a 0.4V signal was induced in it. This signal was transformed up to 4V by

a transformer (figure 7). Since the motor speed was around 50 rotations per second, the period of the pick-up signal would be 20 ms. However, the fastest mechanical counters available within a reasonable price range need a minimum on-and-off time of approximately 20 ms each. It was therefore necessary to put in a decade counter or a 1/10-divider in the circuit for the pick-up signal. This arrangement is shown in figure 7. A differential comparator changes the transformer signal into 4V square waves, and for ten of these pulses coming to the decade counter one new pulse will go out. This one is amplified up to 12V by a transistor and activates relay 3. For each time this happens, the 120V AC circuit to the I.T.T.-counter is closed and one count is registered.

The resistors in the circuits are there in order to get the correct magnitude of current and voltages to the integrated circuits. The purpose of the two capacitors are to short circuit to ground, noise and other disturbances in the signal. The decade counter is especially sensitive; it works up to frequencies of 2 Mc and can therefore pick up signals which are too short to be detected by the oscilloscope that was used to check the circuit.

In the beginning of the experiments this counting arrangement worked perfectly. However, after some time the bearings in the gears and the bending arm started wearing out. The electrical contact between the pressure vessel and

the test piece was not so good any longer, and we got a lot of sparks in the bearings and the gears. This had two effects. First, each spark induced a voltage in the pick-up coil with the result that the counter started working irregularly. Secondly, these sparks deteriorated the oil, it became completely black and smelled bad, and it apparently lost its lubricating power with the result that the ball bearings on the bending arm broke down. It also turned out that small carbon-like particles were formed by the sparks. Under a couple of long runs it happened that these particles settled down on the connector socket for the electrical leads. This resulted in short circuit in the motor's AC supply which then caused the blowing of a fuse. In order to avoid this the oil was changed after each series of runs, and the connector socket was cleaned regularly.

It was also desired to measure the oil temperature during the tests since the motor developed around 20 w of heat. A thermocouple could not be used since it had to be connected to the brass cones; moreover, the contact points would therefore be at the same temperature, and we would not get any voltage out. An ordinary thermometer was therefore used to measure the oil temperature immediately after the test was over and the pressure vessel was opened.

In order to get as low as possible oil temperature, a powerful fan was used to cool the pressure vessel from the

outside. The motor body and the brass cylinder were also perforated with large holes so that the oil could circulate more freely into the vessel wall to help the heat transfer. In all tests, the oil temperature was found to be between 32° and 38°C.

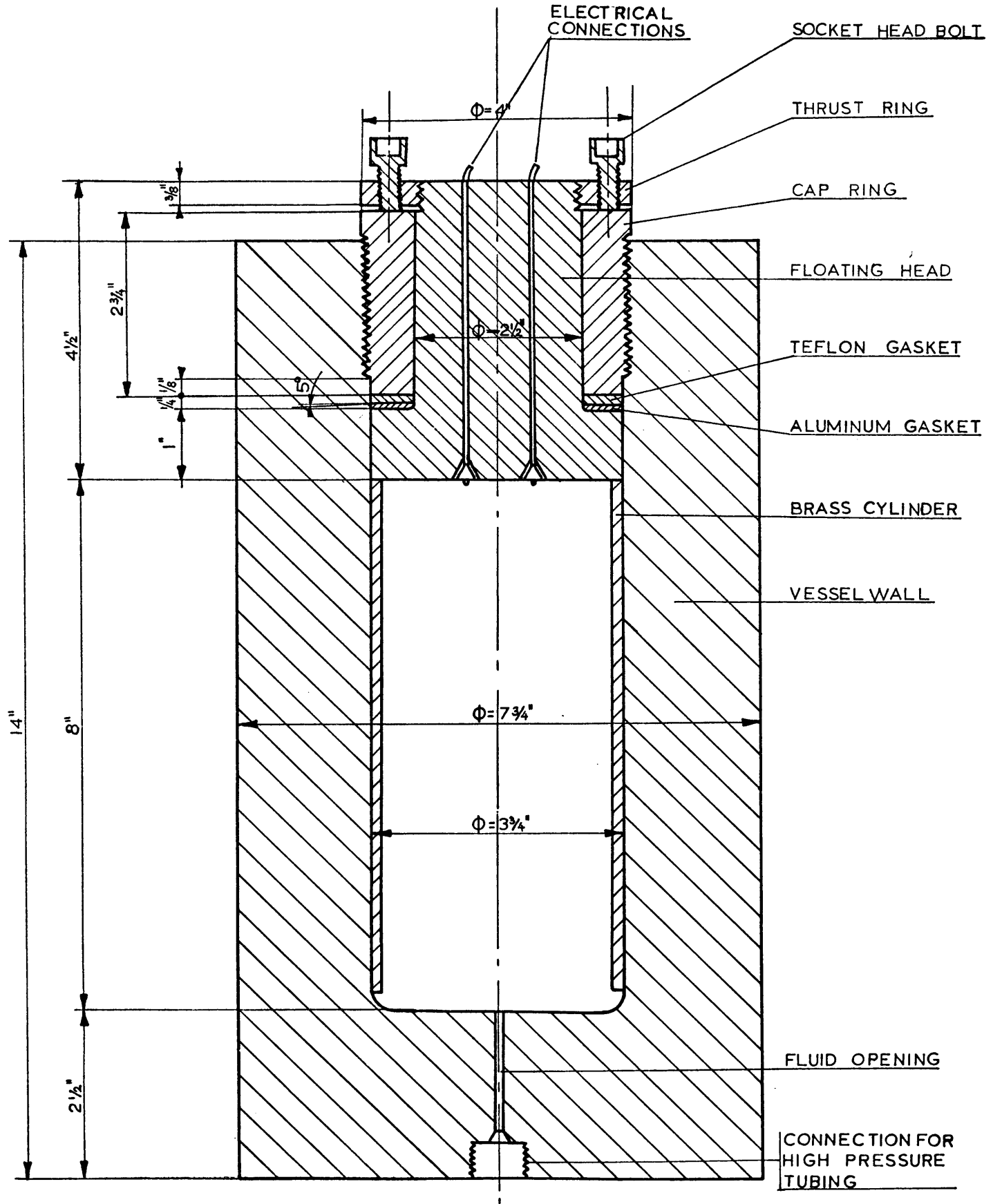


FIGURE 2. PRESSURE VESSEL AND CLOSURE

SCALE 1:2

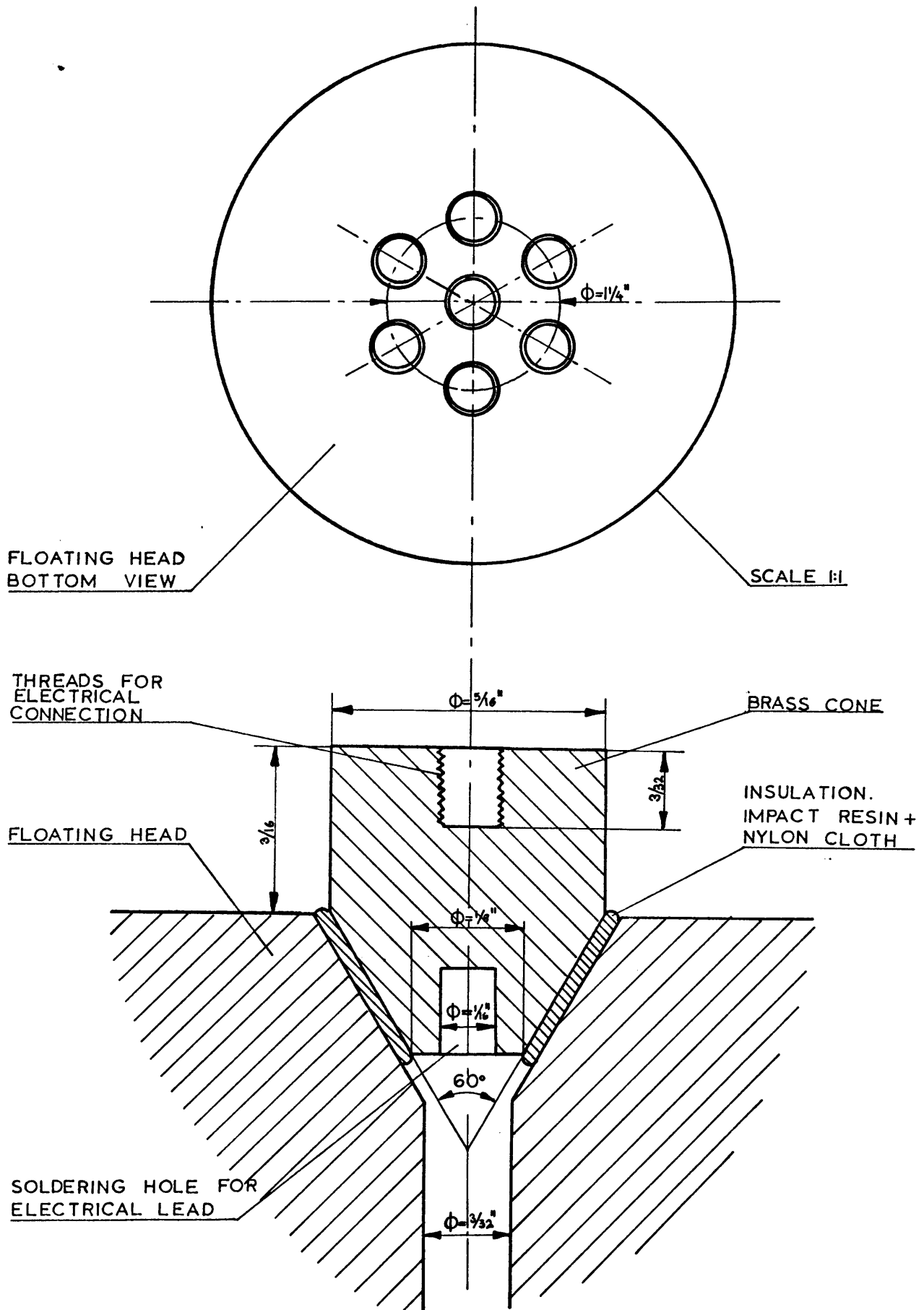


FIGURE 3. CONE CONNECTION FOR ELECTRICAL LEADS

APPROXIMATE SCALE 6:1

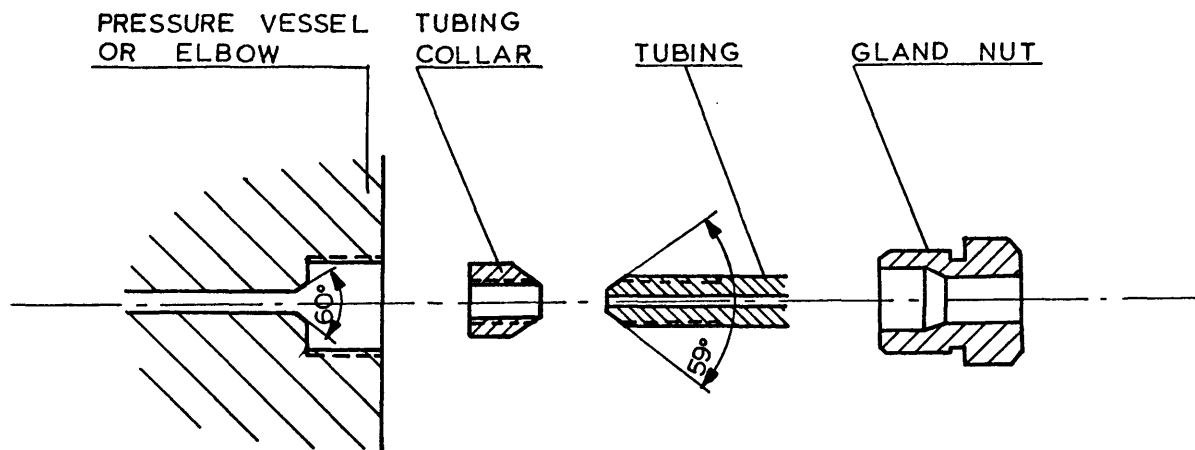


FIGURE 4A. SCHEMATIC VIEW OF CONNECTION FOR HIGH PRESSURE TUBING

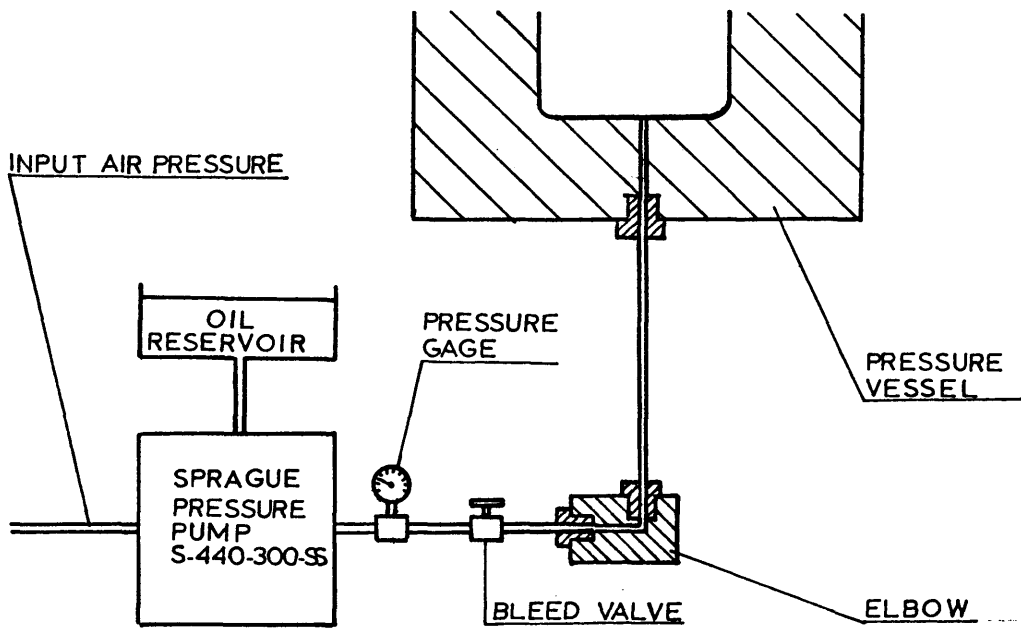


FIGURE 4B. HIGH PRESSURE ARRANGEMENT

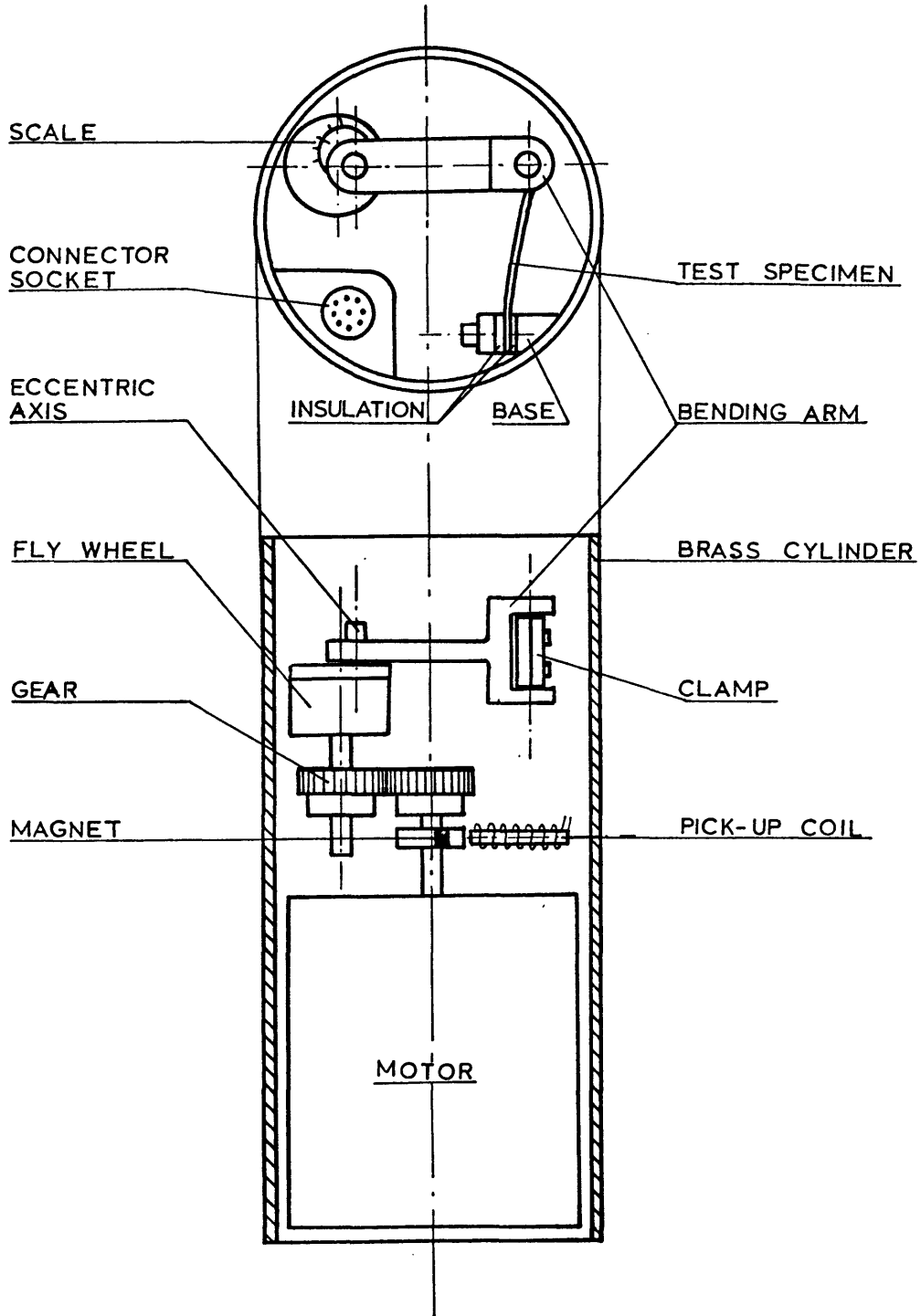


FIGURE 5. SCHEMATIC FIGURE OF THE BENDING MECHANISM

SCALE 1:2

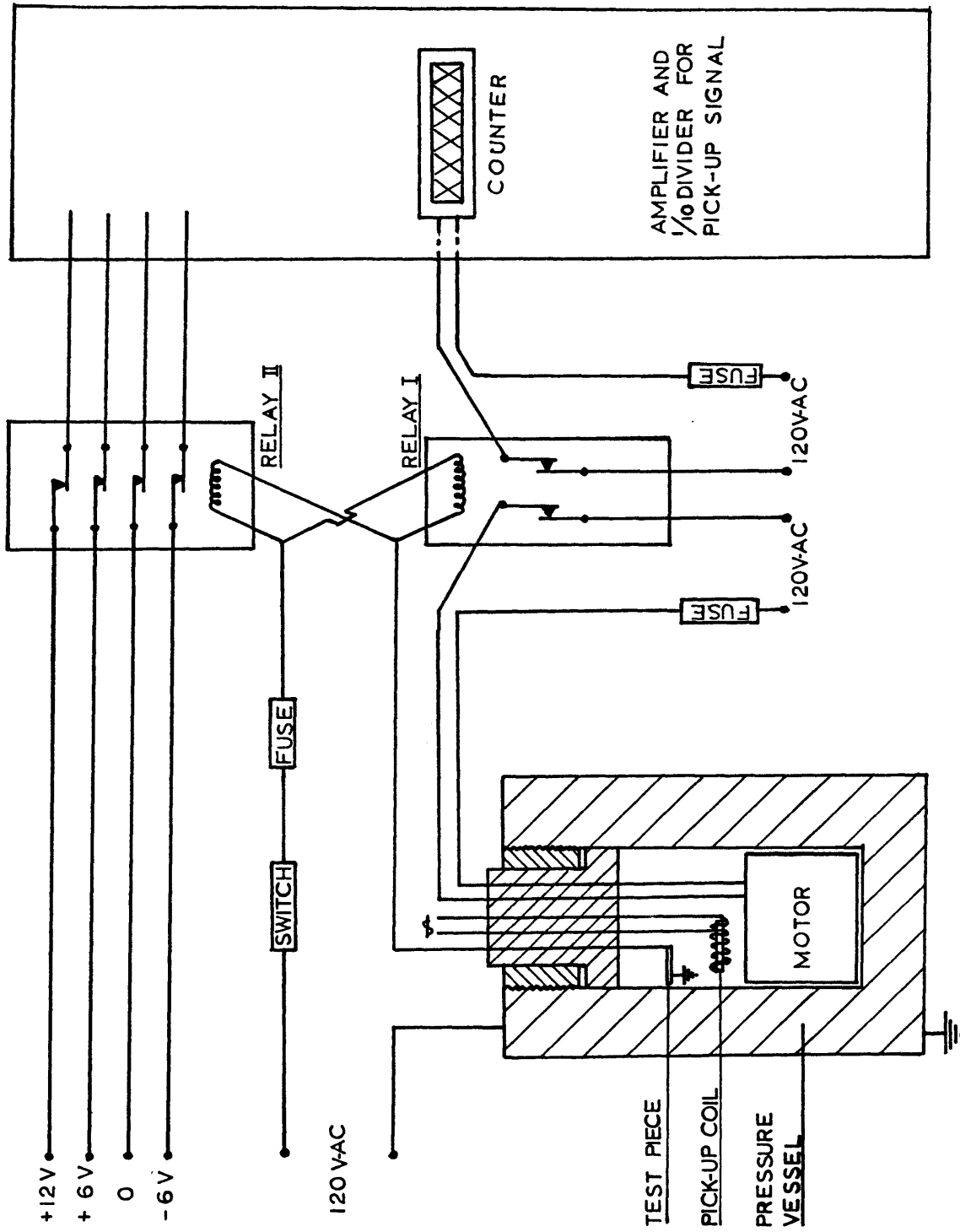


FIGURE 6. SCHEMATIC FIGURE OF THE ELECTRICAL ARRANGEMENT

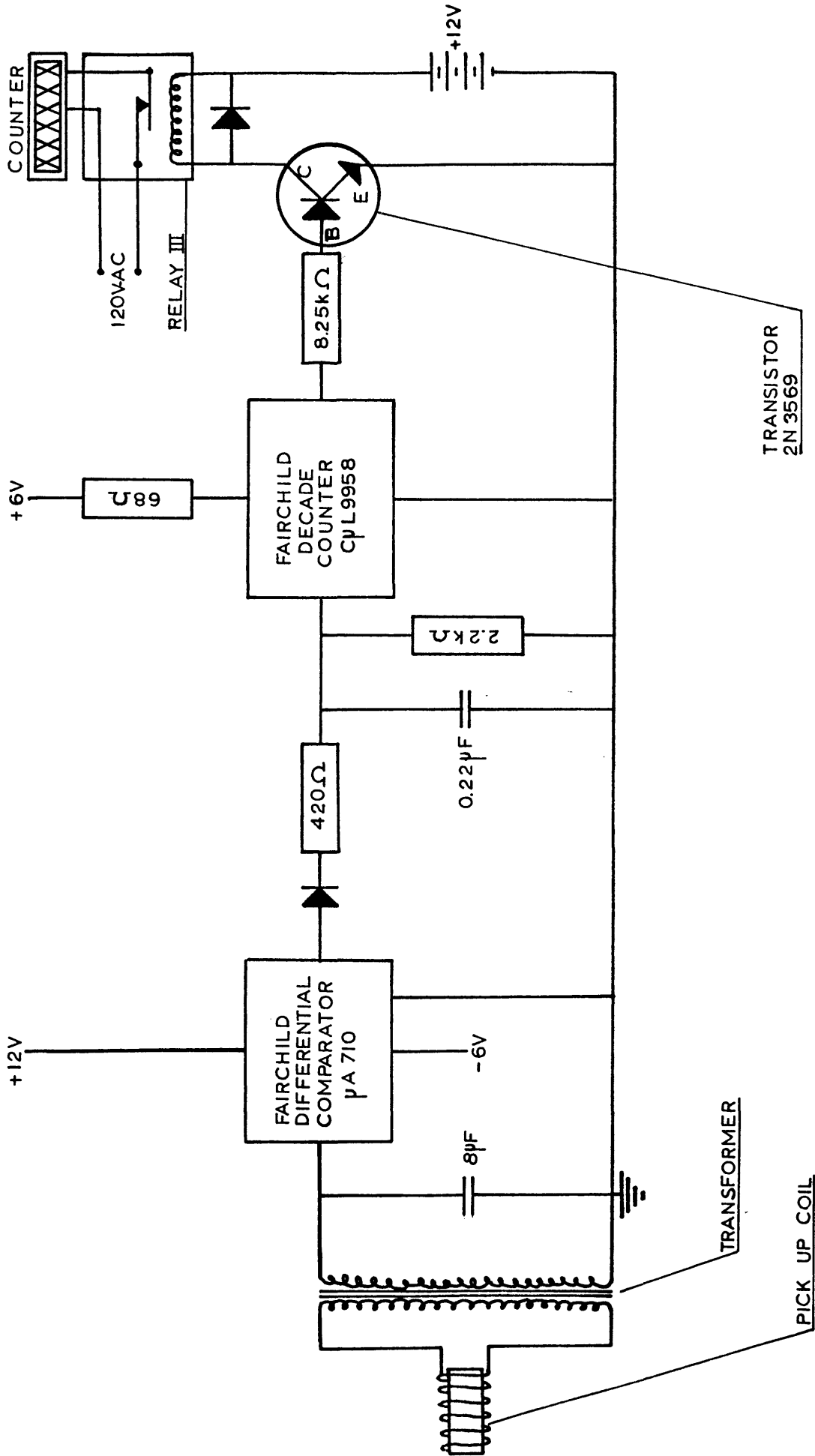


FIGURE 7. SCHEMATIC FIGURE OF THE ELECTRONIC COUNTER

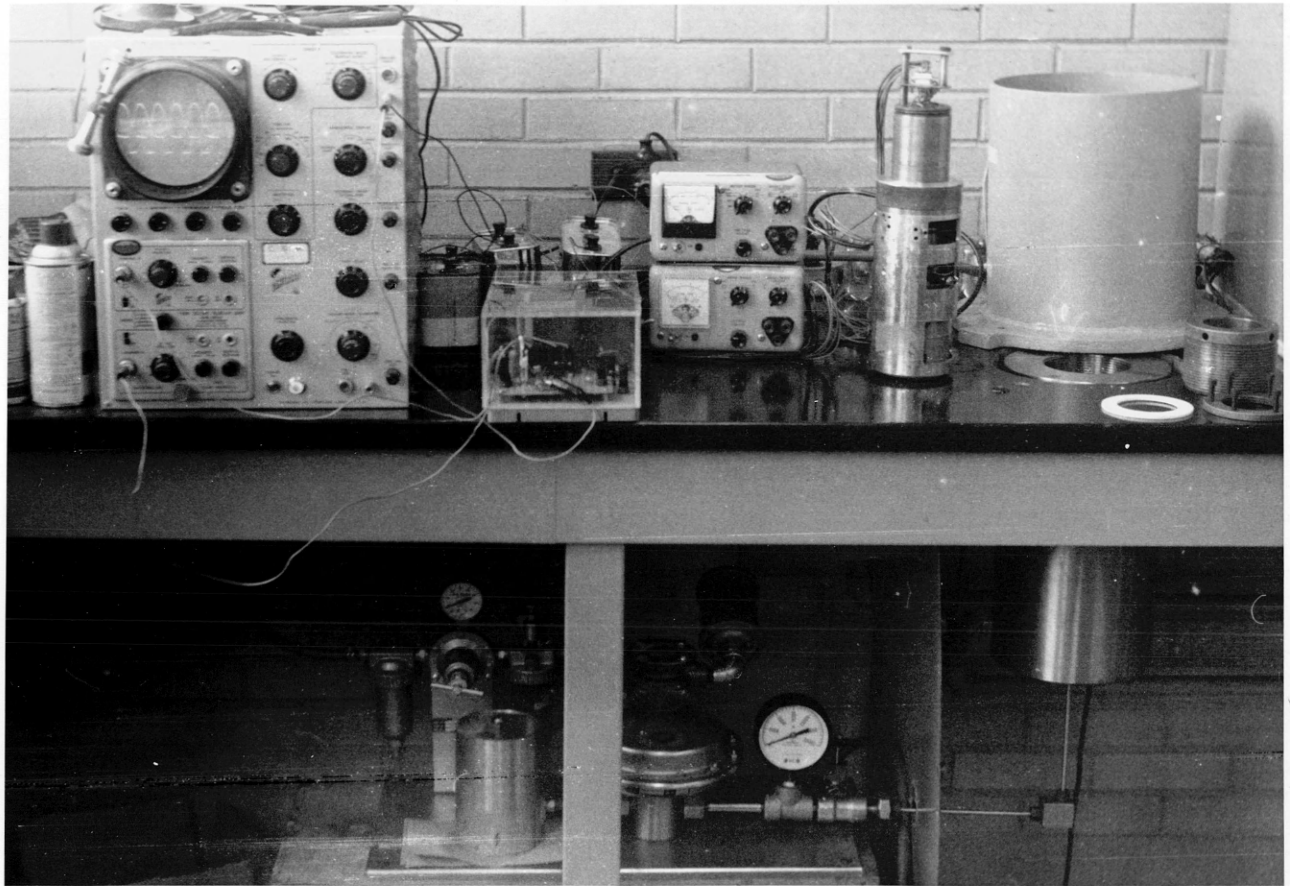


FIGURE 8. GENERAL LAYOUT OF THE APPARATUS

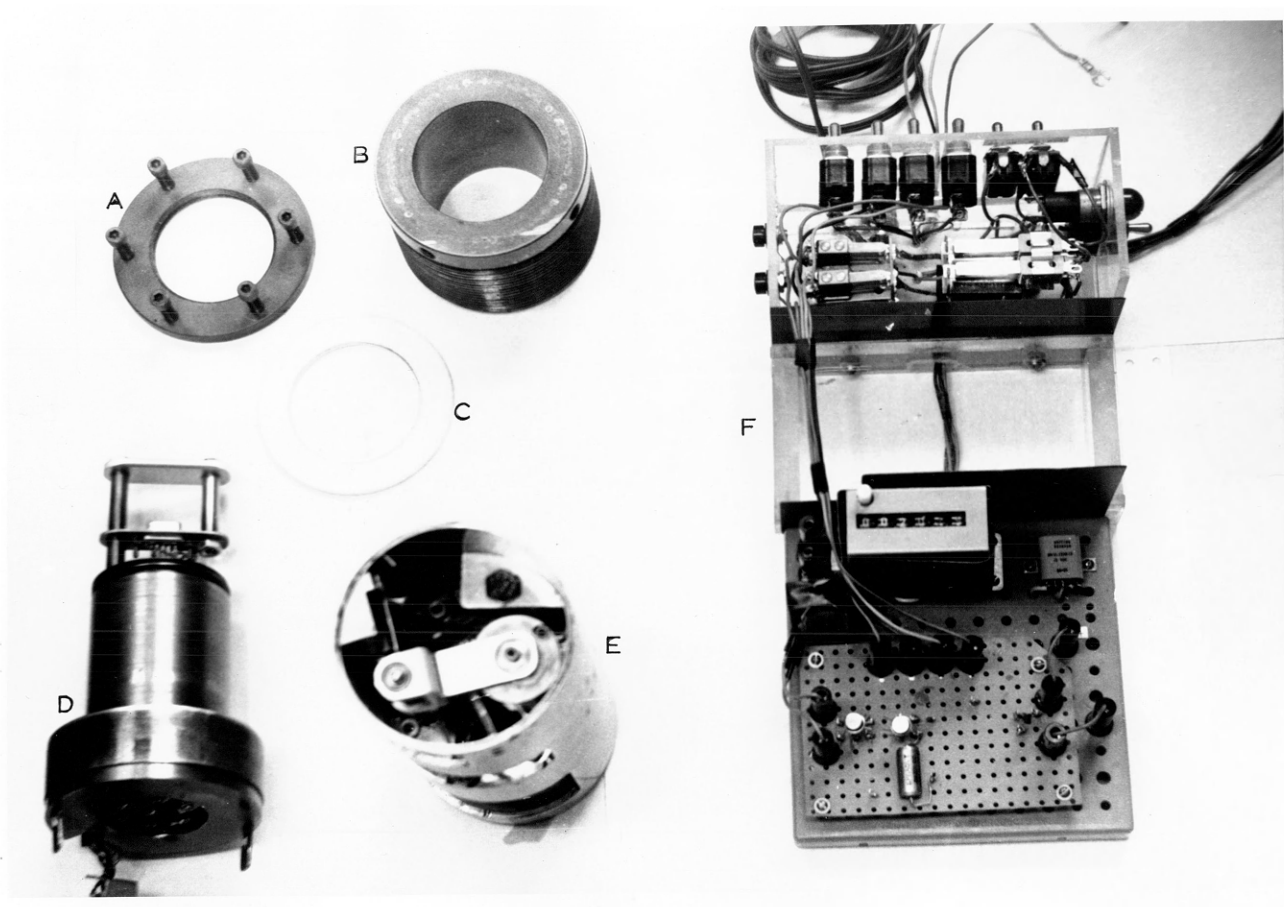


FIGURE 9. DETAIL OF MAIN PARTS OF THE APPARATUS

- A: THRUST RING
- B: CAP RING
- C: TEFLON GASKET
- D: FLOATING HEAD
- E: BRASS CYLINDER WITH BENDING MECHANISM
- F: COUNTING MECHANISM

EXPERIMENTAL RESULTS

A series of fatigue tests was made in oil for three different pressure levels: 14 psi (atmospheric pressure), 5,000 psi, and 10,000 psi. Each series had seven different stress levels. The experimental data from these series are presented graphically in figure 10.

A test series was also run in air at atmospheric pressure, and the fatigue curve obtained was found not to be different from the one obtained with the test piece in oil at the same pressure (figure 11).

Fifteen tests were run in oil at a stress amplitude of 60,500 psi. Five of these were at an oil pressure of 14 psi. Five others were at 14 psi for the first 1500 cycles (the first 5% of expected lifetime if run in air), and thereafter at 10,000 psi for the rest of the lifetime. Finally, five more tests were run at 10,000 for the whole lifetime. These results are presented graphically in figure 12, and numerically in tables 1, 2, and 3.

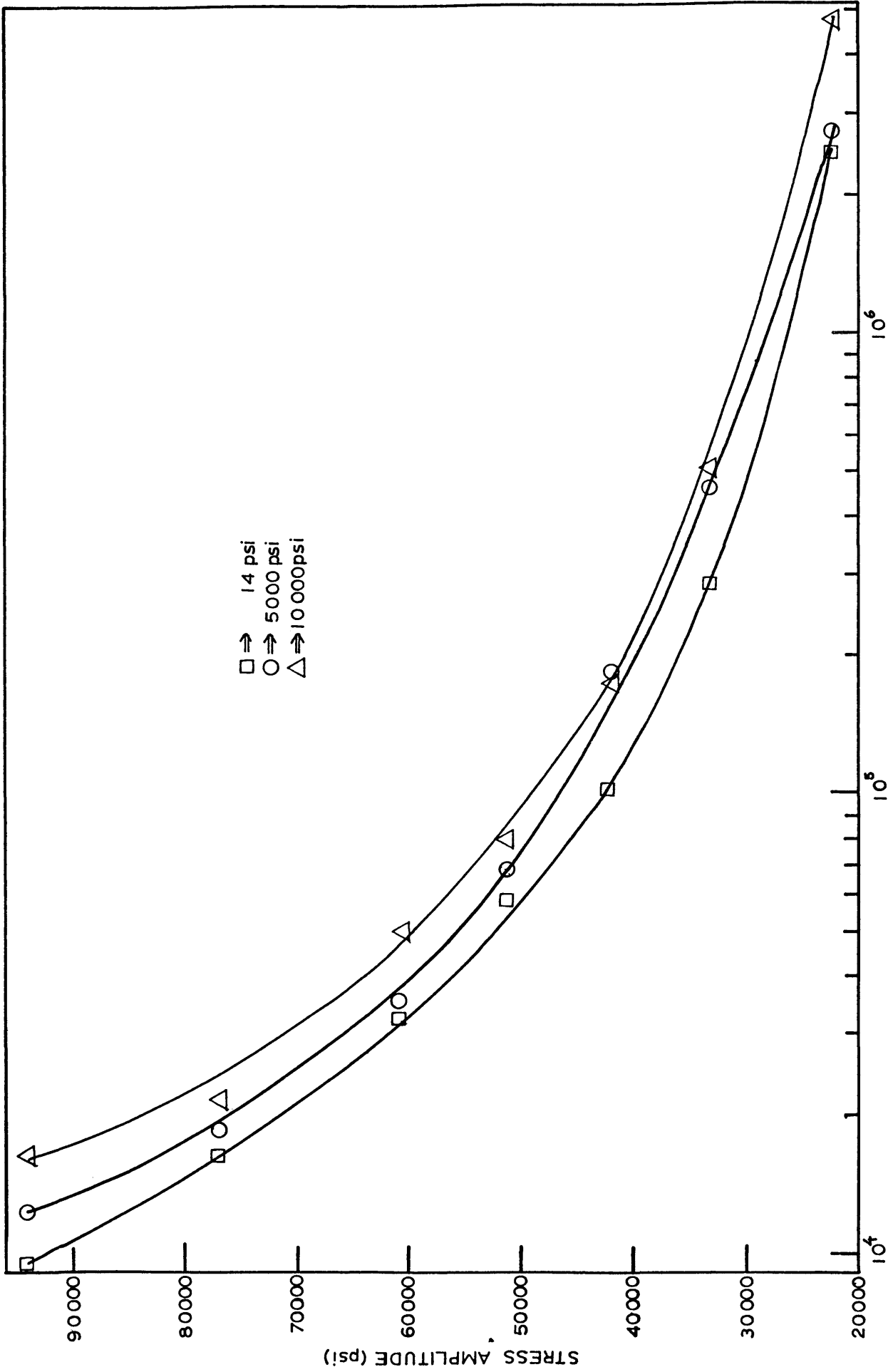


FIGURE 10. RELATION BETWEEN CYCLIC STRESS AND FATIGUE LIFE FOR THE TEST PIECE UNDER THREE DIFFERENT OIL PRESSURES.

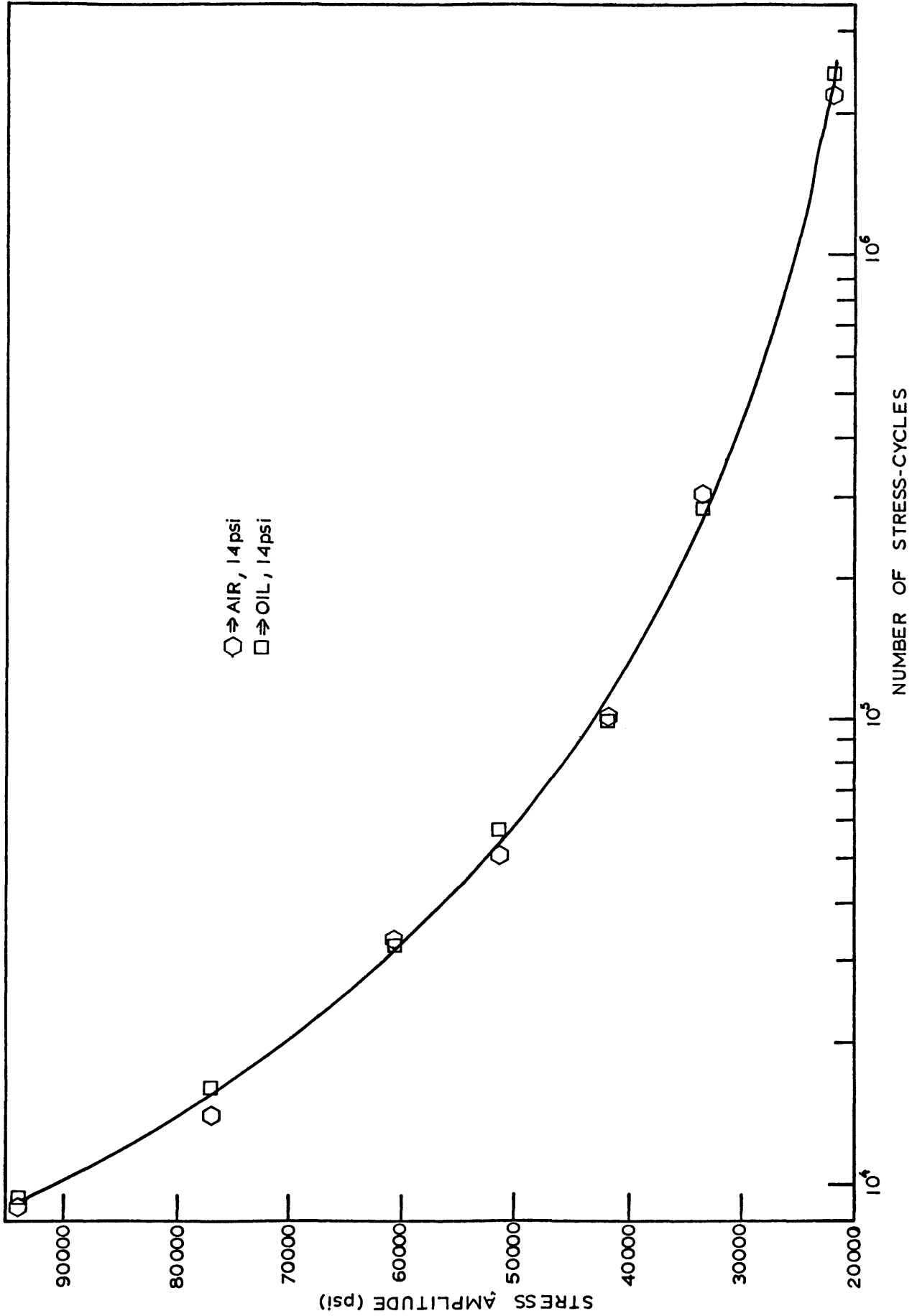


FIGURE II. RELATION BETWEEN CYCLIC STRESS AND FATIGUE LIFE FOR THE TEST PIECE IN AIR AND OIL AT ATMOSPHERIC PRESSURE.

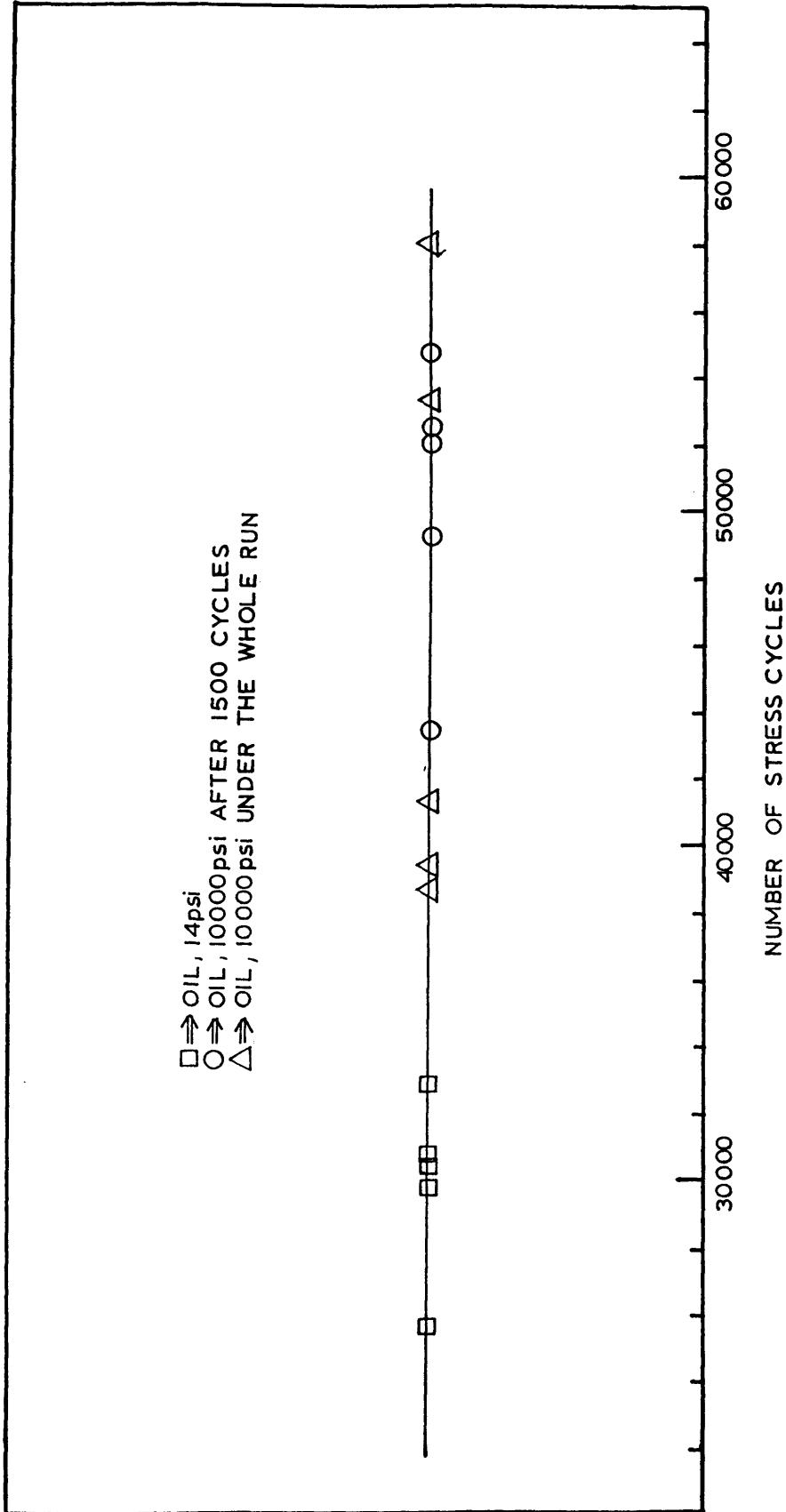


FIGURE 12. LIFETIME OF A TESTPIECE BEING SUBJECTED TO A CYCLIC STRESS OF 60500psi UNDER THREE DIFFERENT PRESSURE COMBINATIONS.

Table 1. Fatigue data for tests in oil under three different pressures. N = fatigue life.

Stress Amplitude (psi)	$N_0, 14\text{psi}$	$N_1, 5000\text{ psi}$	$N_2, 10000\text{psi}$	$\frac{\Delta N_1}{N_0} = \frac{\Delta N_2}{N_0} =$	
				$\frac{N_1 - N_0}{N_0}$	$\frac{N_2 - N_0}{N_0}$
94,000	9,600	12,500	16,600	0.30	0.72
77,000	16,450	18,550	21,330	0.12	0.29
60,500	32,800	35,250	38,880	0.08	0.18
51,000	55,900	68,310	76,200	0.22	0.36
42,000	100,100	184,330	173,700	0.84	0.73
33,000	281,500	458,000	504,700	0.83	0.79
22,000	2,550,000	2,690,000	4,843,700	0.05	0.89
		Mean values		0.34	0.57

Table 2. Comparison of fatigue data in oil and air under atmospheric pressure.

Stress Amplitude (psi)	N_o , oil	N_3 , air	$\frac{\Delta N}{N_o}$
94,000	9,600	9,200	0.04
77,000	16,450	13,350	0.18
60,500	32,800	33,000	-0.01
51,000	55,900	51,000	0.08
42,000	100,100	101,000	-0.01
33,000	281,500	302,000	-0.07
22,000	2,550,000	2,200,000	<u>0.13</u>
		Mean value =	0.015 = 1.5 percent

Standard deviation

$$S = \sqrt{\frac{\sum_{i=1}^7 \left(\frac{\Delta N}{N_o} \right)_i - \frac{\Delta \bar{N}}{N_o} \right)^2}{6}} = 0.10$$

Table 3. Fatigue-data for tests in oil at a 60,500 psi stress amplitude.
 N_1 = fatigue life in oil, 14 psi
 N_2 = fatigue life in oil, 10,000 psi
 N_3 = fatigue life for specimens being subjected to 14 psi pressure in the first 1500 cycles and 10,000 psi for the rest of the lifetime.

	<u>N_1</u>	<u>N_2</u>	<u>N_3</u>
	30,270	38,440	54,480
	30,360	53,100	43,200
	25,630	41,780	49,180
	29,910	60,100	52,400
	32,800	38,800	52,060
Mean values, $\bar{N}_i =$	<u>29,800</u>	<u>46,444</u>	<u>50,264</u>
Standard deviation $S_i =$	<u>5,014</u>	<u>9,682</u>	<u>8,754</u>

DISCUSSION OF EXPERIMENTAL RESULTS

The fatigue data obtained show that there is a significant increase in the lifetime of a specimen when the hydrostatic pressure is increased from 14 psi to 5,000 and 10,000 psi. From table 1 we see that with respect to the lifetime of a test piece in oil under atmospheric pressure, the fatigue life has increased with an average of 34 percent at 5,000 psi and 57 percent at 10,000 psi oil pressure. This result agrees with those obtained by Rowland, DeVries and Gibbs (1967, p. 131), who made rotating beam fatigue tests for pressures up to 100,000 psi, and with Burns and Parry's results (1964, p. 293). They made torsion fatigue tests under an oil pressure of 40,000 psi and found an increase of 30-40 percent in the lifetime.

In table 2 it is shown that the average lifetime was relatively 1.5 percent higher in oil than in air, both at 14 psi pressure. However, in Appendix III it is shown that from a few simple assumptions and at a 95 percent significance level, one can conclude that there is no difference in the fatigue lives of the specimens under these two test conditions. That is, one can conclude that the oil itself or the combination of oil and adsorbed air in it have no positive or negative effect on the lifetime of the samples.

Considering the test series which were run at 60,500 psi stress level, we see that the tests run at atmospheric pressure for the first 1500 cycles and then at 10,000 psi for the remaining lifetime had an average lifetime which was not significantly different from the value obtained for samples run under 10,000 psi for the whole lifetime. And its mean was more than two standard deviations from the mean of the samples run under atmospheric pressure only. After what was said in the theory we can then conclude that at this pressure level the hydrostatic pressure has its main effect on the propagation of cavities and microcracks. However, it might also have an effect on the vacancy concentration, the diffusion of vacancies and the formation of pores, but this can not be detected because of the scattering of the data. Rowland, DeVries, and Gibbs (1967, p. 131), who made similar experiments with Fe, Al, and Ni-wires at pressures around 100,000 psi, concluded from their data that the nucleation of cracks exhibits a much stronger pressure dependence than the propagation of cracks. However, the large difference in pressure may explain why the present investigation could not detect this effect.

SUMMARY AND CONCLUSIONS

An apparatus for fatigue under high hydrostatic pressure was designed and built. It was tested successfully with oil as the pressure medium and for pressures up to 10,000 psi. Reverse bending fatigue tests were run with cold rolled copper samples. From the data obtained the following conclusions could be made:

1. There was a significant increase in the lifetime of the specimens when the hydrostatic pressure was increased to 5000 and 10,000 psi. The increase in lifetime with respect to the lifetime of a test piece in oil under atmospheric pressure was around 34 and 57 percent, respectively.
2. The increase in lifetime was mainly due to a slowing down of the propagation of cavities and microcracks by the hydrostatic pressure.
3. Under atmospheric pressure there was no difference in lifetime for test pieces ran in oil compared to those ran in air.

SUGGESTIONS FOR IMPROVING THE
APPARATUS AND FOR FURTHER WORK

One basic change is recommended on the apparatus. Instead of using an electrical circuit through the bending arm and the test piece in order to find out when the test piece breaks, it would be better to use a microswitch close to the bending arm so that when the test piece breaks the arm will bump into the switch and thereby turn off the current to the relay for the counter and the motor circuits. This must be a one-way microswitch so that the relay current will not be turned on again if the arm bumps into it several times.

It could also be useful to have a thermostat and a heating element inside the pressure vessel so that the equilibrium temperature for long runs, 39°C, could be held for shorter runs also.

For further work it may be suggested that materials other than copper should be tested. Especially steels and other alloys having inclusions, foreign particles and a second phase may strongly show a pressure dependence on their mechanical behavior. Tests should be made to determine whether any of these materials exhibit any irreversible effects after being subjected to a hydrostatic pressure of

around 10,000 psi for different periods of time. The ultimate goal should be to make fatigue tests under high hydrostatic pressure, with a corrosive liquid like sea water as a pressure medium.

Appendix I: Calculation of Stresses in the Test Specimen

In a repeated bending test the test piece is supported in one end and bent up and down in the other end. This bending amplitude can easily be measured using a dial gage, and we will then need to know the relationship between the deflection of the test piece and the stresses set up in it.

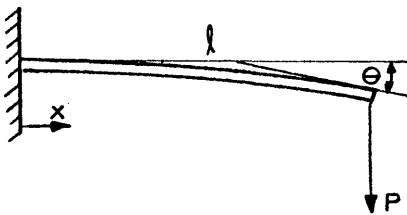


Figure 13

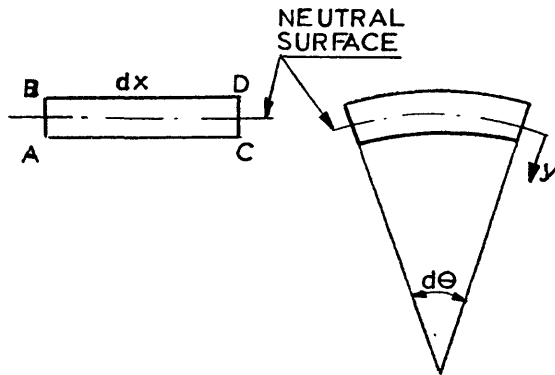


Figure 14

Let us consider a test piece of length l as shown in figure 13. It is supported on one end and a force P is applied to the other end. Its cross-section is rectangular with thickness h and width b . Figure 14 shows a small section dx before and after bending. Before bending, the two planes AB and CD are parallel. After bending, the angle between the two planes is $d\theta$. The plane in the middle of the test piece which is not subjected to any strain is called the neutral surface. Its radius of curvature is ρ and is given by

$$\rho d\theta = dx \quad (5)$$

or

$$\frac{d\theta}{dx} = \frac{1}{\rho} \quad (6)$$

From figure 14 it can be seen that any segment at a distance y from the neutral surface elongates by the amount $yd\theta$.

Therefore, the strain in the x-direction is:

$$\epsilon_x = - \frac{yd\theta}{dx} = - \frac{y}{\rho} \quad (7)$$

For the stress in the x-direction we get

$$\sigma_x = - Ey \frac{1}{\rho} \quad (8)$$

where E is the elastic modulus of the test piece.

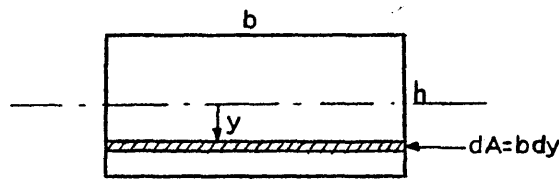


Figure 15.

A cross-section of the test piece perpendicular to the x-axis is shown in figure 15. The stress on the small cross-section area dA exerts a moment about the neutral axis which is given by

$$dM = \sigma_x dAy \quad (9)$$

Integrating over the whole cross-section, this moment must

be equal to the external applied moment in order to have equilibrium:

$$M = \int_A \sigma_x y dA = - \frac{E}{\rho} \int y^2 dA = - \frac{EI}{\rho} \quad (10)$$

where I is the moment of inertia about the neutral axis. For a rectangular cross-section this is equal to $bh^3/12$. Substituting for ρ in equation 8, we get the following expression for the stress in the x-direction:

$$\sigma_x = \frac{M}{I} y = - \frac{P(\ell-x)y}{\frac{bh^3}{12}} \quad (11)$$

The bending moment M is defined to be negative when we have bending downwards. Thus, we get the following stress-distribution on a cross-section perpendicular to the x-axis:

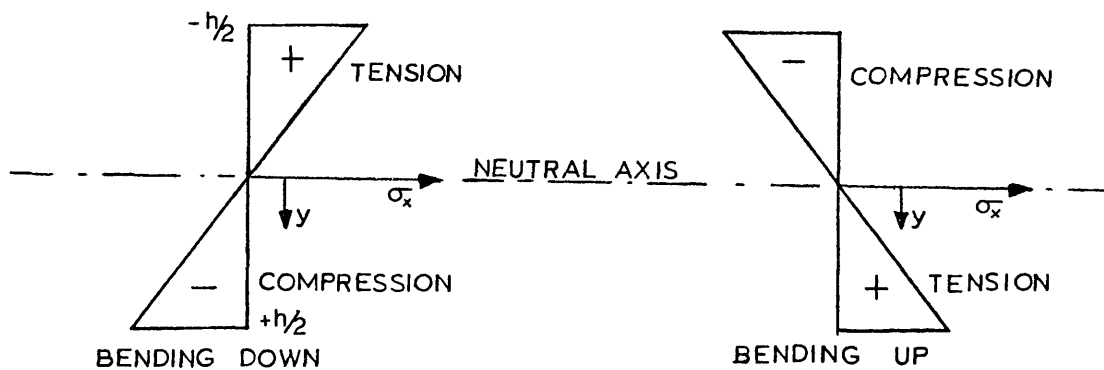


Figure 16.

The maximum stress is produced in the fibers furthest away from the neutral axis. In a reverse bending, the stress will vary sinusoidally, compression in one half period and

tension in the other half.

From equation 11 it can be seen that if the test piece has a width which vary as

$$b(x) = b_0 \left(\frac{l-x}{l} \right) \quad (12)$$

there will be a constant stress in this section equal to

$$\sigma_x = - \frac{12 P l y}{b_0 h^3} \quad (13)$$

The test piece was designed in this way as shown in figure 17 (scale 2:1).

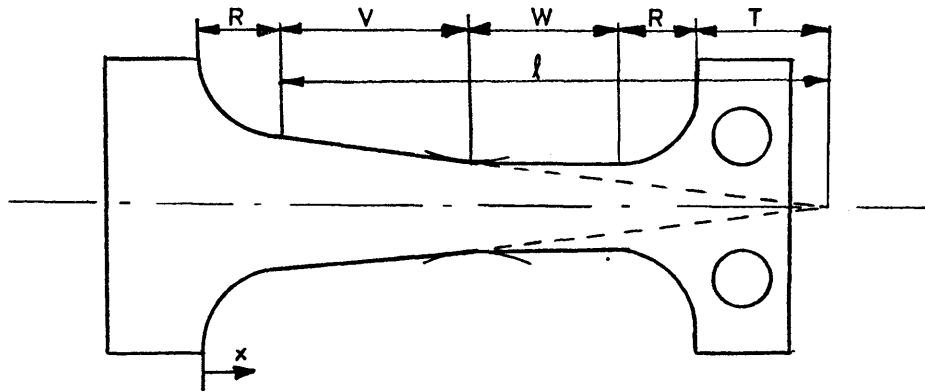


Figure 17.

The force is applied at the apex A of the triangle formed by extending the sides of the tapered test section. That is, the axis of the bending arm goes through this point. Thus, we have constant stress in the test piece between $x = R$ and $x = R + v$. There will be less stress in the other parts of the test piece so we will expect it to brake in this tapered section.

Having the given design, it is then left to find the relationship between the bending amplitude and the applied force P , the latter is needed in order to calculate the stress from equation 13. Combining equations 6 and 10 we have

$$\frac{d\theta}{dx} = - \frac{M}{EI} \quad (14)$$

The angle θ is approximately given by (figure 13)

$$\theta = \frac{dy}{dx} \quad (15)$$

Thus, substituting into equation 14, we get the following differential equation giving the relationship between the deflection y and the distance x from the point of support for the test piece.

$$\frac{d^2y}{dx^2} = - \frac{M}{EI} = \frac{P(\ell-x)}{E \frac{b(x)h^3}{12}} \quad (16)$$

Therefore, for small deflections the angle θ between the x -axis and the tangent to the test piece section at $x = \ell$ is given by

$$\theta = \frac{dy}{dx} = \int_0^{\ell} \frac{P(\ell-x)}{E \frac{b(x)h^3}{12}} \quad (17)$$

The deflection δ at $x = \ell$ is given by

$$\delta = \int_0^{\ell} \int_0^{x'} \frac{P(\ell-x)dx dx'}{E \frac{b(x)h^3}{12}} \quad (18)$$

The calculations of the angle θ and the deflection δ must be

carried out separately for each section of the test piece having different width $b(x)$ (figure 18).

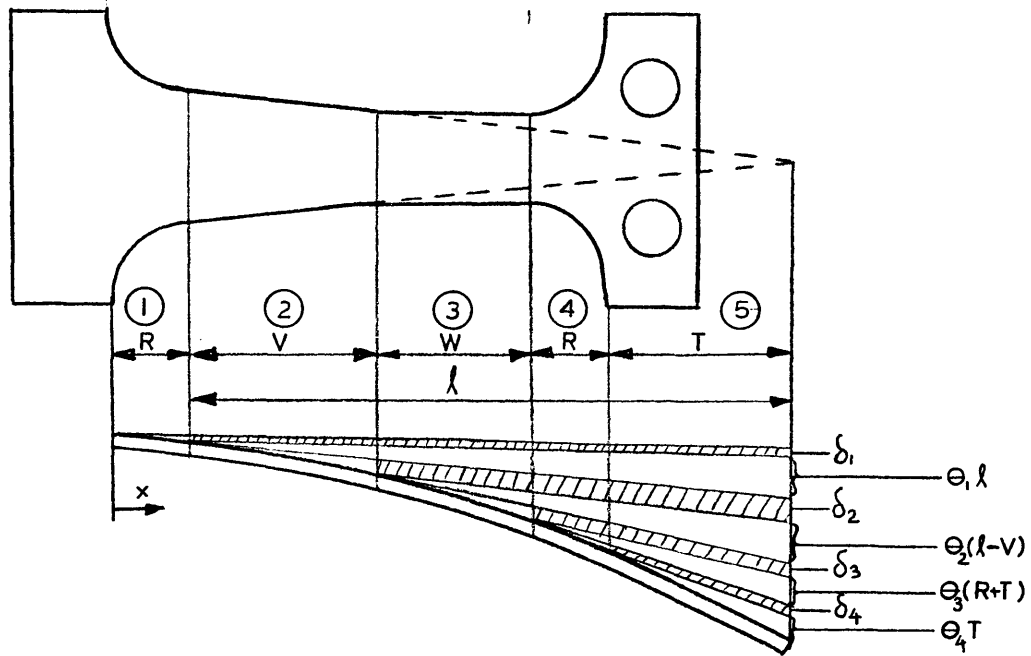


Figure 18.

There are five sections with different $b(x)$, and from the figure it can be seen that the final deflection is given by

$$\delta = \delta_1 + \delta_2 + \delta_3 + \delta_4 + \theta_1 l + \theta_2(l-V) + \theta_3(R+T) + \theta_4 T \quad (19)$$

For the different sections the width is given by:

Section 1

$$b(x) = b_0 + 2(R - R \sin \phi)$$

or
$$b(x) = b_0 + 2(R - \sqrt{2Rx - x^2}) \quad (20)$$

Section 2

$$b(x) = b_0 \left(\frac{l+R-x}{l} \right) \quad (21)$$

Section 3

$$b(x) = b_o \left(\frac{l-V}{l} \right) \tag{22}$$

Section 4

$$b(x) = b_o \left(\frac{l-V}{l} \right) + 2(R - R \cos \phi)$$

or

$$b(x) = b_o \left(\frac{l-V}{l} \right) + 2(R - \sqrt{R^2 - (x - (R+V+W))^2}) \tag{23}$$

Unfortunately, using the differential equation 16 one can solve for δ and θ only for the sections 2 and 3. The $b(x)$ values for section 1 and 4 mean that the equation cannot be solved analytically. However, using Simpson's integration formula one can find θ_1 and θ_4 . Since this formula can be used to make simple integrations only, and not double, approximations had to be done in order to calculate δ_1 and δ_4 . This was done in the following way:

Section 1

Section 2

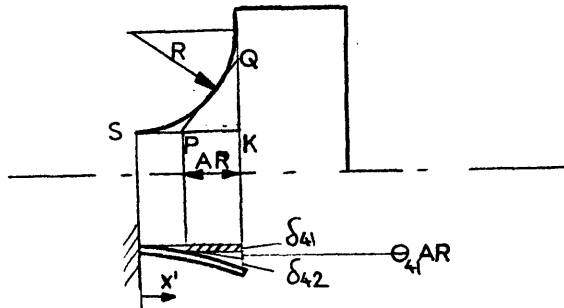
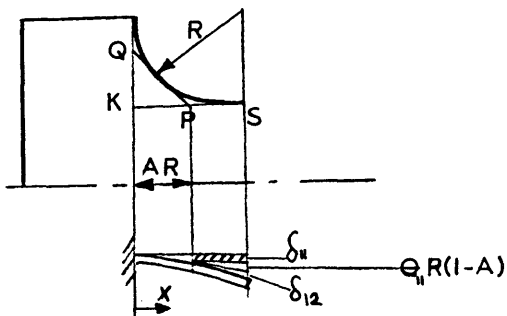


Figure 19

Figure 20

Instead of letting the section width $b(x)$ vary as a circle segment with radius R , it is approximated with the two straight lines QP and PS . The constant A determining the line PQ is chosen so that the area PQK is equal to the area under the circle segment. That is,

$$\frac{1}{2} (AR)^2 = R^2 - \pi R^2/4 \quad (24)$$

This equation yields $A = 0.65$. Thus, dividing section 1 into two new sections as shown on figure 19 we get for the deflection δ_1 :

$$\delta_1 = \delta_{11} + \delta_{12} + \theta_{11} \cdot (1-A)R \quad (25)$$

For section 1 the width is given by:

$$b(x) = b_0 + 2(AR-x) \quad \text{for} \quad 0 < x < AR \quad (26)$$

$$b(x) = b_0 \left(\frac{\ell + R - x}{\ell} \right) \quad \text{for} \quad AR < x < R \quad (27)$$

For section 4 the deflection is given by

$$\delta_4 = \delta_{41} + \delta_{42} + \theta_{41} AR \quad (28)$$

and the width for this section is

$$b(x) = b_0 \left(\frac{\ell - V}{V} \right) \quad \text{for} \quad 0 < x' < R(1-A) \quad (29)$$

$$b(x) = b_0 \left(\frac{\ell - V}{V} \right) + 2(x' - R + RA) \quad \text{for} \quad R(1-A) < x' < R \quad (30)$$

All these $b(x)$ values give analytical expressions for δ and θ when equation 16 is integrated.

Thus, the final expression for the deflection is given by

$$\begin{aligned} \delta = & \delta_{11} + \delta_{12} + \delta_2 + \delta_3 + \delta_{41} + \delta_{42} + \theta_{11}(1-A)R + \theta_1 \ell \\ & + \theta_2(\ell - V) + \theta_3(R + T) + \theta_4 T + \theta_{41} AR \end{aligned} \quad (31)$$

The mathematical expression for each of these terms is found to be:

$$\delta_{11} = \frac{6P}{Eh^3} \left[\frac{(RA)^2}{2} + (\ell + R(1-A) - \frac{b_o}{2})(RA - (2RA + \frac{b_o}{2}) \ln(1 + \frac{2RA}{b_o})) \right] \quad (32)$$

$$\delta_{12} = \frac{12P\ell}{Eb_o h^3} \left[\frac{(R(1-A))^2}{2} \right] \quad (33)$$

$$\delta_2 = \frac{12P\ell}{Eb_o h^3} \left[\frac{V^2}{2} \right] \quad (34)$$

$$\delta_3 = \frac{12P\ell}{Eb_o h^3 (\ell - V)} \left[(\ell - V) \frac{W^2}{2} - \frac{W^3}{6} \right] \quad (35)$$

$$\delta_{41} = \frac{12P\ell R^2 (1-A)^2}{Eb_o h^3 (\ell - V)} \left[\frac{R}{3} + \frac{RA}{6} + \frac{T}{2} \right] \quad (36)$$

$$\delta_{42} = \frac{6P}{Eh^3} \left[-\frac{(RA)^2}{2} + (T + RA + \frac{b_o(\ell - V)}{2\ell})(-RA + (RA + \frac{b_o(\ell - V)}{2\ell}) \cdot \ln(1 + \frac{2RA}{b_o(\frac{\ell - V}{\ell})})) \right] \quad (37)$$

$$\theta_{11}(1-A)R = \frac{6PR(1-A)}{Eh^3} \left[RA + (\ell + R(1-A) - \frac{b_o}{2}) \ln(1 + \frac{2RA}{b_o}) \right] \quad (38)$$

$$\theta_{1\ell} = \frac{12P\ell}{Eb_o h^3} \frac{R \int_0^R \frac{(\ell + R - x) dx}{1 + \frac{2}{b_o}(R - \sqrt{2Rx - x^2})}} \quad (39)$$

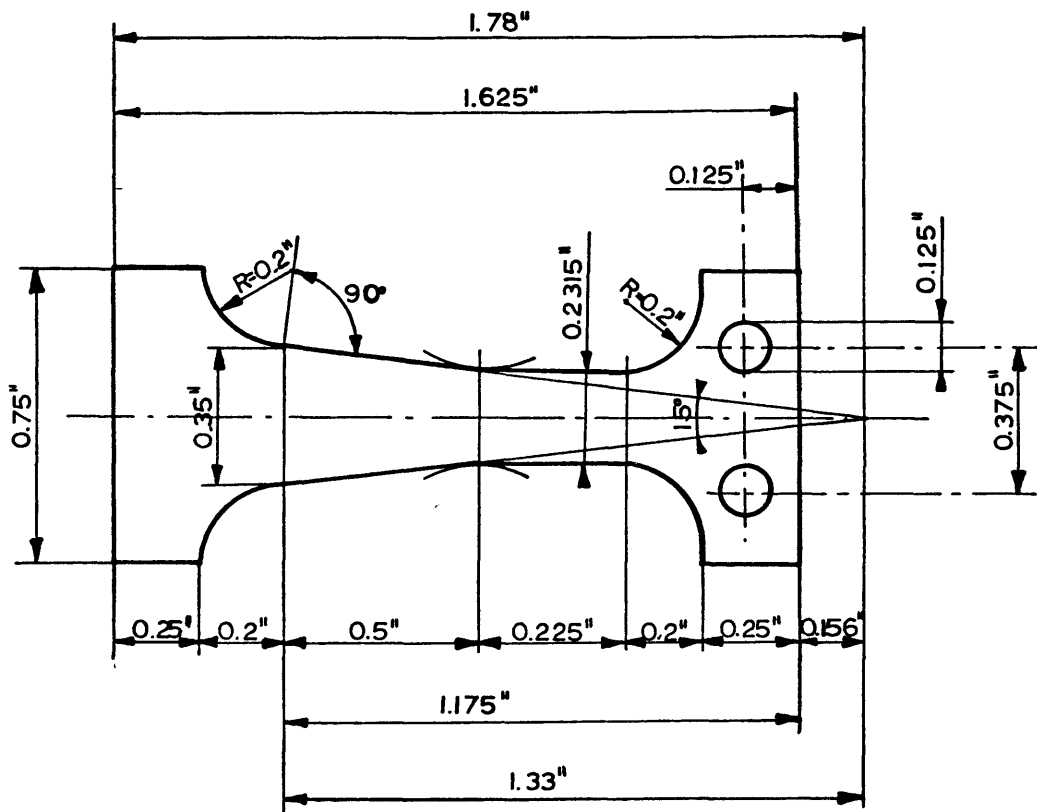
$$\theta_2(\ell - V) = \frac{12P\ell(\ell - V)V}{Eb_o h^3} \quad (40)$$

$$\theta_3^{(R+T)} = \frac{12P\ell(R+T)}{Eb_o h^3(\ell-V)} \left[\ell W - \frac{W^2}{2} - VW \right] \quad (41)$$

$$\theta_4^T = \frac{12PT}{Eb_o h^3} \int_0^R \frac{(R+T-x) dx}{\frac{\ell-V}{\ell} + \frac{2}{b_o} (R - \sqrt{R^2-x^2})} \quad (42)$$

$$\theta_{41}^{RA} = \frac{12P\ell R(1-A)RA}{Eb_o h^3(\ell-V)} \left[\frac{R}{2} + \frac{RA}{2} + T \right] \quad (43)$$

All these calculations were carried out numerically on the computer, and the relationship between the deflection and the applied force was found. Knowing the latter, the stress in the x-direction could be computed from equation 11. In this way the linear relationship between the deflection and maximum stress in the test piece was found as shown in figure 22.



TEST PIECE THICKNESS = 0.0434"

SCALE 2:1

FIGURE 21. TEST PIECE

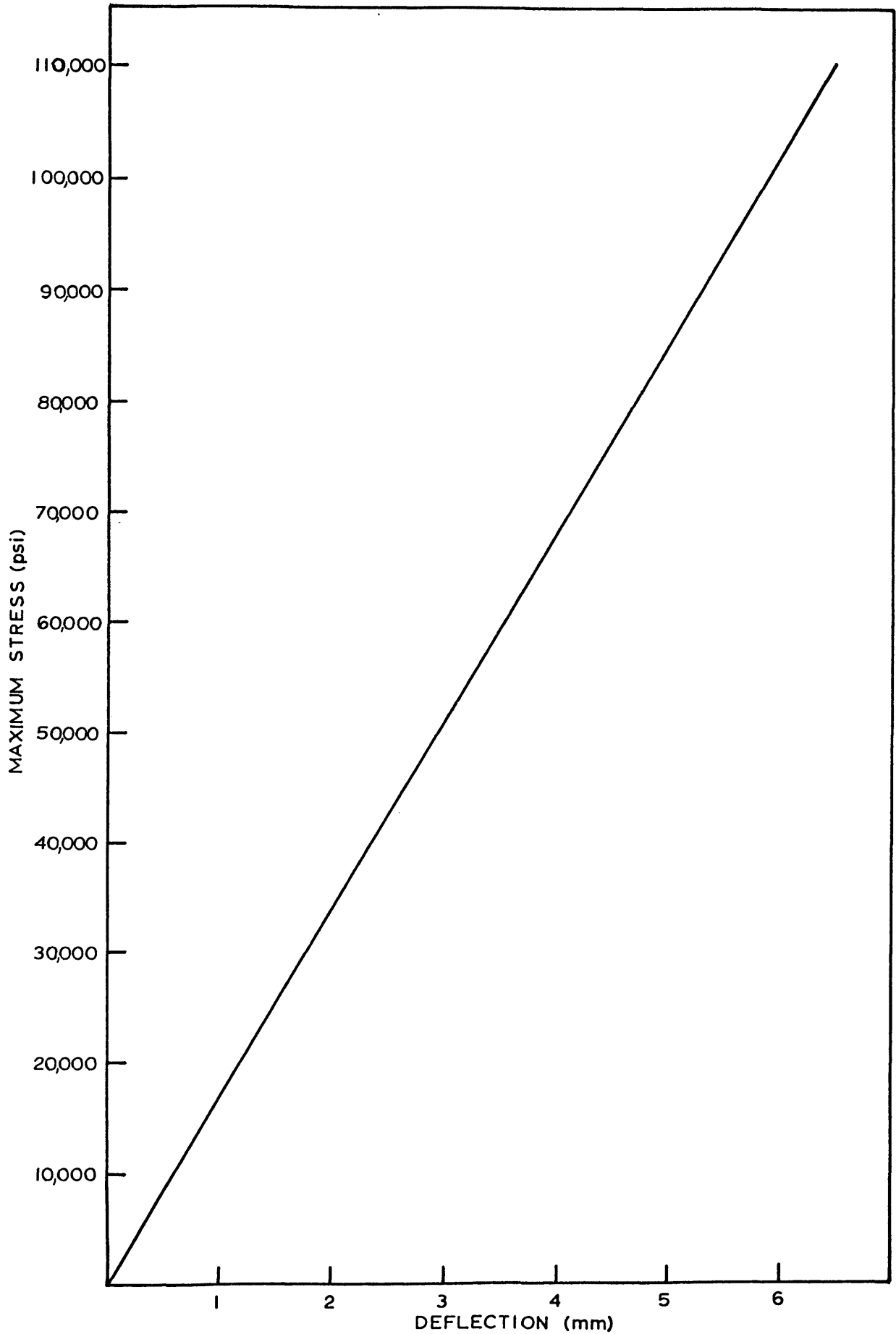


FIGURE 22. RELATION BETWEEN MAXIMUM STRESS AND DEFLECTION FOR A COPPER TEST PIECE

Appendix II: Design of the Pressure Vessel

For the construction of the pressure vessel, it was convenient to use an 8-in.-diameter bar of 302 stainless steel, which was available on campus. In annealed form this steel has the following properties (ASME Handbook, 1954, p. 56):

Yield strength, 0.2% offset: 35-40,000 psi

Tensile strength : 80-90,000 psi

Having this in mind the following calculations were done in order to find the stresses set up in a thick-walled cylinder (Comings, 1956, p. 160):

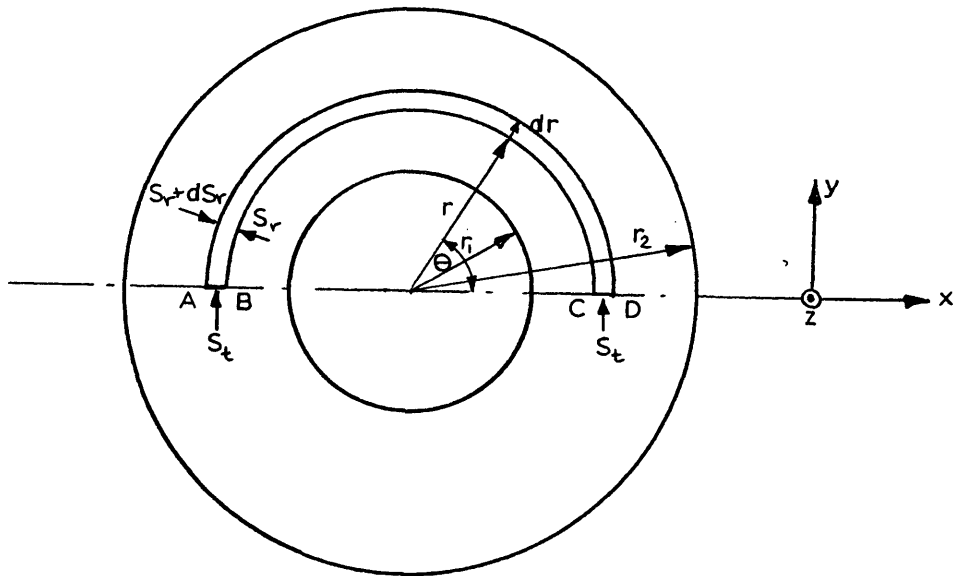


Figure 23.

We will consider a section of a thick-walled cylinder as shown in the figure. The cylinder length perpendicular to the paper plane along the z-axis is equal to one unit. The following notations will be used:

r = radius

r_1 = inner radius of the cylinder

r_2 = outer radius of the cylinder

p_1 = pressure inside the cylinder

p_2 = pressure outside the cylinder

S_r = radial stress

S_t = tangential stress

S_z = longitudinal stress

ϵ_z = longitudinal strain

E = modulus of elasticity

G = modulus of rigidity

ν = Poisson's ratio

θ = angle between r and the x-axis

The half ring ABCD which lies between r and $r + dr$ is in equilibrium, and the sum of all forces acting in y-direction must therefore be zero. These forces are:

On the inner surface

$$F_1 = \int_0^{\pi} S_r r d\theta \sin\theta = 2rS_r \quad (44)$$

On the outer surface

$$F_2 = -2(r+dr)(S_r+dS_r) \quad (45)$$

On the sections AB and CD

$$F_3 = F_4 = S_t dr \quad (46)$$

When these forces are added together and the sum is set equal to zero, the following equation is obtained after some calculations:

$$-S_t + \frac{d}{dr} (S_r r) = 0 \quad (47)$$

Assuming constant longitudinal components of stress and strain throughout the wall, Hook's law can be written as

$$\frac{S_z - E\varepsilon_z}{\nu} = S_r + S_t = C_1 \quad (48)$$

where C_1 is a constant. This can be rewritten as

$$S_t = C_1 - S_r \quad (49)$$

Substituting this expression in equation 47, we get

$$S_r + \frac{d}{dr} (S_r r) = C_1 \quad (50)$$

With the introduction of the new variable

$$S_r = \frac{C_2}{r^2} \quad (51)$$

where C_2 is a constant, the general solution of equation 50 is found to be

$$S_r = \frac{C_2}{r^2} + \frac{C_1}{2} \quad (52)$$

The two constants are determined from the following boundary conditions:

$$\begin{aligned} S_r &= -p_1 & \text{for } r &= r_1 \\ S_r &= -p_2 & \text{for } r &= r_2 \end{aligned} \tag{53}$$

We then get:

$$S_r = \frac{p_1 - p_2 \kappa^2 - (p_1 - p_2) \left(\frac{r_2}{r}\right)^2}{\kappa^2 - 1} \tag{54}$$

where $\kappa = r_2/r_1$. Since $p_2 \gg p_1$, this equation can be written as

$$S_r = \frac{-p_1 \left(\frac{r_2}{r}\right)^2 - 1}{\kappa^2 - 1} \tag{55}$$

Substituting for S_r and C_1 in equation 49, we get the following expression for the tangential stress

$$S_t = \frac{p_1 \left(\left(\frac{r_2}{r}\right)^2 + 1\right)}{\kappa^2 - 1} \tag{56}$$

The variation of these two stresses with the radius is shown on figure 24:

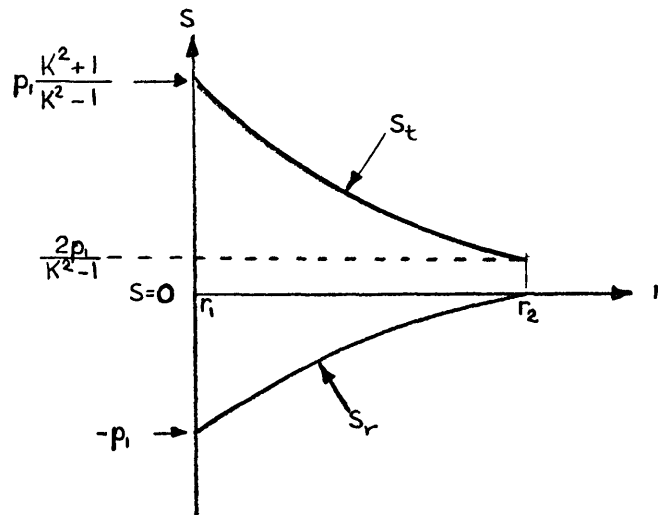


Figure 24.

We see that we get maximum stresses in the inner wall.

These are given by

$$\begin{aligned} S_r(r=r_1) &= -p_1 \\ S_t(r=r_1) &= p_1 \frac{\kappa^2+1}{\kappa^2-1} \end{aligned} \quad (57)$$

Since the pressure vessel is cylinder-like and closed at both ends, we get the following longitudinal stress:

$$S_z = \frac{p_1 \pi r_1^2}{\pi(r_2^2 - r_1^2)} = \frac{p_1}{\kappa^2-1} \quad (58)$$

The vessel was designed so that $\kappa = 2$ (figure 2). With this value the expression for the stresses becomes

$$\begin{aligned} S_r &= -p_1 \\ S_t &= 1.66 p_1 \\ S_z &= 0.33 p_1 \end{aligned} \quad (59)$$

All these calculations are done under the assumption of perfectly elastic deformation of all parts of the cylinder. We have three principal stresses in the cylinder, and we need to know how high an internal pressure we might have without reaching the point where we start getting plastic deformation. The information we have about 302 stainless steel is that its yield point is at least 35,000 psi. That is, this is the yield point in a simple tensile test with stress in one direction only. There are several theories predicting the limit of elastic action when three principal stresses are present, and only the data from a simple tension

test are available. Of these theories, the one accepted as the most reliable (Comings, 1956, p. 178) is von Mises' maximum energy of distortion theory (Nadai, 1931, p. 72). This one can be developed in the following way:

When we operate within the elastic range, the stored energy per unit volume is given by

$$W = \frac{1}{2}(S_1\epsilon_1 + S_2\epsilon_2 + S_3\epsilon_3) \quad (60)$$

Using Hook's law and substituting for ϵ_1 , ϵ_2 , and ϵ_3 , we get

$$W = \frac{1}{2E} [S_1^2 + S_2^2 + S_3^2 - 2\nu(S_1S_2 + S_2S_3 + S_3S_1)] \quad (61)$$

This is the total energy of elastic deformation. The hydrostatic pressure in the metal is given by

$$S_H = \frac{1}{3} (S_1 + S_2 + S_3) \quad (62)$$

Therefore, the elastic energy due to a change in volume is

$$W' = \frac{1}{2} S_H(\epsilon_1 + \epsilon_2 + \epsilon_3) = \frac{1}{6}(S_1 + S_2 + S_3)(\epsilon_1 + \epsilon_2 + \epsilon_3) \quad (63)$$

On application of Hook's law, this equation gives us

$$W' = \frac{1-2\nu}{6E} [S_1^2 + S_2^2 + S_3^2 + 2(S_1S_2 + S_2S_3 + S_3S_1)] \quad (64)$$

Thus, the stored elastic energy used in changing the shape per unit volume, or the energy of distortion is

$$\begin{aligned} U = W - W' &= \frac{1}{6G} [S_1^2 + S_2^2 + S_3^2 - (S_1S_2 + S_2S_3 + S_3S_1)] \\ &= \frac{1}{12G} [(S_1 - S_2)^2 + (S_2 - S_3)^2 + (S_3 - S_1)^2] \end{aligned} \quad (65)$$

where G is the modulus of rigidity and is given by

$$G = \frac{E}{2(1+\nu)} \quad (66)$$

In simple tension only S_1 is non-zero, and when we have reached the limit of elastic behavior $S_1 = S_y$. As equation 65 is valid under any stress combination, we then have for the energy of distortion under simple tension

$$U = \frac{S_y^2}{6G} \quad (67)$$

Von Mises assumed that the energy of distortion had a constant value given by equation 67. Therefore, when equating the equations 65 and 67, we get the condition for yielding when three principal stresses are present:

$$(S_1 - S_2)^2 + (S_2 - S_3)^2 + (S_3 - S_1)^2 = 2S_y^2 \quad (68)$$

Using the three principal stresses given by equation 59 in this equation, we get the following expression for the internal pressure:

$$p_1 = 0.433 S_y \quad (69)$$

Since the yield stress is 35,000 psi, we get $p_1 = 15,200$ psi. That is, for this internal pressure we will reach the limit of elastic behavior for the metal in the inner part of the cylinder wall.

Appendix III: Statistical Treatment of Fatigue Data in Air
and Oil Under Atmospheric Pressure

From table 2 it can be seen that the average lifetime was relatively 0.015 higher in oil than in air, both at 14 psi pressure. The standard deviation for these observations was 0.10. In order to see if this difference in lifetime is significant, the following assumptions will be made:

- The relative difference in lifetime is a normal, independent random variable.
- The true difference is zero.
- The standard deviation of the mean lifetime is $0.10/7 = 0.038$.

Using these assumptions, we will make a 95 percent confidence interval for the observed mean.

$$P_r \left[\left(\frac{\overline{\Delta N}}{N_o} \right) < A \right] = 0.95 \quad (70)$$

where A is a constant we will determine. We can change this expression to

$$P_r \left[\frac{\left(\frac{\overline{\Delta N}}{N_o} \right) - 0}{0.038} < \frac{A - 0}{0.038} \right] = 0.95 \quad (71)$$

From our assumptions, the term on the left side of the inequality sign is normally distributed with a mean equal to zero and a variance equal to one. From tables for the normal distribution (Johnson, Leone, p. 460) we find that

$$\frac{A}{0.038} = 1.64 \quad (72)$$

That is, $A = 0.062$. Since our observed mean value is well within this limit, we can conclude from our assumptions and at a 95 percent significance level that there is no difference in the fatigue lives of specimens run in air or in oil when both are under atmospheric pressure. Therefore, the oil itself or the combination of oil and adsorbed air in it have no positive or negative effect on the lifetime of the samples.

BIBLIOGRAPHY

- ASME Handbook: Metals properties, 1954: McGraw-Hill Book Company, 433 p.
- Asai, G., and Hayes, E. T., 1957, Ductile chromium: American Society of Metals, p. 138.
- Bridgman, P. W., 1952, The physics of high pressure: G. Bell and Sons, Ltd., London, 445 p.
- Bullen, F. P., Henderson, F., Hutchinson, M. M., and Wain, H. L., 1964, The effect of hydrostatic pressure on yielding in iron: Phil. Mag., v. 9, p. 285-297.
- Bullen, F. P., Henderson, F., Wain, H. L., and Paterson, M.S., 1964, The effect of hydrostatic pressure on brittleness in chromium: Phil. Mag., v. 9, p. 803-815.
- Burns, D. J., and Parry, J. S. C., 1964, Effect of large hydrostatic pressure on the torsional fatigue strength of two steels: Journal of Mech. Engr. Sci., v. 6, no. 3, p. 293-307.
- Comings, E. W., 1956, High pressure technology: McGraw Hill Book Co., New York, 572 p.
- DeVries, K. L., Baker, G. S., and Gibbs, P., 1963, Pressure dependence of the creep of lead: J. Appl. Phys., v. 34, no. 8, p. 2254-2257.
- Findley, W. N., and Tracy, J. F., 1966, Fatigue under pulsating hydrostatic pressure: Proc., 1st Intl. Conf. Fract., Yokobon, Kawasaki and Swedlow Eds., Jap. Soc. for Strength and Fract. of Met., p. 1479-1491.
- Galli, J. R., and Gibbs, P., 1964, The effect of hydrostatic pressure on the ductile-brittle transition in molybdenum: Acta Metallurg., v. 12, p. 775-778.
- Johnson, N. L., and Leone, F. C., 1964, Statistics and experimental design: John Wiley and Sons, v. 1, 523 p.
- Kochendorfer, A., 1954, Arch. Eisenhüttenw. no. 25, p. 351.

- Nadai, A., 1931, Plasticity: McGraw Hill Book Co., New York, 349 p.
- Proceedings, 1st Intl. Conf. Fract., 1966, Yokobori, Kawasaki and Swedlow Eds., Jap. Soc. for Strength and Fract. of Met.
- Rowland, S. C., DeVries, K. L., and Gibbs, P., 1967, The effect of pressure on fatigue: Intl. J. of Fract. Mech., v. 3, no. 2, p. 131-144.
- Shewmon, P. G., 1963, Diffusion in solids: McGraw-Hill Book Company, New York, 203 p.
- Sines, G., and Waisman, J. L., 1959, Metal fatigue: McGraw Hill Book Company, New York, 415 p.
- Timoshenko, S., and Young, D. H., 1962, Strength of materials: D. van Nostrand Company, Inc., Princeton, N.J., 373 p.
- Weertman, J., 1965, The Peach-Koeler equation modified for hydrostatic pressure: Phil. Mag., v. 11, p. 1217-1223.
- Weertman, J., and Weertman, J. R., 1964, Elementary dislocation theory: The MacMillan Co., New York, 213 p.
- Wood, W. A., Cousland, S. Mc K., and Sargant, K. R., 1963, Systematic microstructural changes peculiar to fatigue deformation: Acta Metallurgica, v. 11, p. 643-652.